

Internal wave analysis of recent LOCO measurements in the Mozambique channel

Tycho Huussen
thuussen@nioz.nl

January 23, 2006

Abstract

This study looks at internal wave motions in the most recent data from Long-term Ocean Climate Observations (LOCO) in the Mozambique channel. The seawater flow through the channel has been monitored from November 2003 until March 2005, using seven moorings with sixteen current meters and six ADCP's in total. Data from these instruments shows strong intermittent signals at the tidal frequencies and in the near-inertial wave band. In this report we focus on internal near-inertial waves. Possible generation sources of these waves have been identified. Eddies develop on a regular basis in this part of the ocean and we have looked into the effect of eddy vorticity on the near-inertial wave band. Preliminary results on the propagation internal inertial wave beams were obtained. The results make clear that a specific design of measurements is required for proper internal wave observation.



Mentor: Dr. L.R.M. Maas
Royal Netherlands Institute for Sea Research

Contents

1	Introduction	3
2	Observations	4
3	Near-inertial waves	9
3.1	Introduction	9
3.2	Generation	9
3.3	Interaction with eddies	13
3.4	Energy and phase	17
3.5	Propagation	17
4	Reflection at boundaries	19
5	Discussion	20
A	Raw data	23
A.1	current meter data	23
A.2	ADCP data	23
B	Slided powerspectra	27
C	ADCP phases and energies at inertial frequency	30
D	Filtered data	34
D.1	Zonal velocity (u)	34
D.2	Meridional velocity (v)	38
E	Hodographs	41
F	Vertical current	45
F.1	Vertical velocity	45
F.2	Vertical spectra	49
G	Extra tables	52

1 Introduction

Why this research? This research is carried out during a parttime internship at Royal NIOZ Texel. In the period from August 2005 till January 2006 I have been working for two days a week at the institute with these objectives:

- get acquainted with physical oceanography,
- explore relevant research questions and
- learn about research methods.

I have a background in experimental physics (UvA, 2004), so I am familiar with scientific research, but frankly, the oceanographic part was completely new to me. Attempting to bridge this gap I read some introductory material on the subject. Analysing real data also taught me a lot about oceanography and at the same time I learned how to use MATLAB. Joining Maarten Buijsman on two Marsdiep measurement sessions gave me some feel of the oceanographic fieldwork. Although I suffered a bit from sea sickness I really enjoyed working at sea. So, unsurprisingly, I am very excited about joining the LOCO¹ cruise to the Mozambique channel in February.

What are we looking at? At the start of the internship Leo Maas and I formulated the following research question:

What is the spatial behaviour of internal waves in the Mozambique channel?

The spatial behaviour of internal waves is especially interesting with regard to ‘internal wave attractors’ [1] [2]. Maas et al. have observed wave attractors in the laboratory, but the phenomenon has not been observed in the ocean yet. The geometry of the Mozambique channel is in principle suitable for wave attractors. Nevertheless, chances that a proper attractor will build up in the channel are slight, because of all kinds of disturbances, like topographic roughness and largely unknown conditions at the ‘open’ sides of the channel.

Several attempts to find internal wave attractors ‘in the wild’ have been undertaken by researchers at NIOZ (e.g. [3] and [4]). In 2003 Manders et al. performed the first studies on internal waves in the Mozambique channel [4]. Analysis of semidiurnal internal tides showed qualitative agreement with model calculations [5], giving some idea of how internal tides may have propagated. However, the observation of wave attractors appeared to be out of scope, since observations lacked spatial resolution to actually ‘see’ wave packets propagate. In contrast to Manders et al. we will pay little attention to internal tides and focus on near-inertial internal waves instead.

Traditional internal wave theory (e.g. [6] and [7]²) describes internal waves ranging from the inertial frequency to the Brunt-Väisälä frequency. The inertial

¹LOCO: Long-term Ocean Climate Observations.

²A nice introduction to internal waves and solitons in Dutch can be found in [8].

oscillation, with frequency f , depends on the rotation of the Earth (Ω) and on latitude (ϕ), according to $f = 2\Omega \sin \phi$. At the location of our measurements, $\sim 17^\circ\text{S}$, we have $f \approx -0.59$ cycles per day (cpd).

In this report we will look at near-inertial waves and semidiurnal internal tides. The semidiurnal lunar tide M_2 has a frequency of 1.93 cpd. Of course we observe a persistent presence of tides throughout the entire mooring period. Tides provide a mechanism for the generation of baroclinic internal tides, which will be regarded in §4. Near-inertial waves are less consistently present in the ocean. However, in some time intervals the frequency band around f is actually more energetic than in the internal tidal wave band. In general most internal wave energy is contained in the inertial and the semidiurnal frequency band. In §3.2 we will identify two periods with increased inertial wave activity and we will suggest a generation source.

2 Observations

In November 2003 sixteen vector measuring current meters and six Acoustic Doppler Current Profilers (ADCP) were deployed in the Mozambique channel, as part of the LOCO program. Seven moorings were deployed at the smallest cross-section of the channel (Fig. 1). The instruments were recovered in March 2005. All current meters worked properly, one ADCP close to the Madagascar shelf was completely damaged and another recorded only 7 bins [9]. ADCP data were averaged over 25 meters by M. Schouten³, giving about 20 bins per ADCP and 106 bins in total. Although the LOCO program was intended for the detection of low-frequency currents (ocean circulation), data have been recorded at rates ranging from 900-1800 seconds. Actually, the sampling rate is sufficient for the observation of internal waves as we intent to do in this report.

In the stratified ocean there is a buoyancy force and an individual water packet will oscillate according to the Brunt-Väisälä frequency N ,

$$N^2 = -\frac{g}{\rho_*} \frac{d\rho_0}{dz}, \quad (1)$$

where g is gravitational acceleration, ρ_* and ρ_0 are average- and local density and z is depth. We have calculated⁴ the Brunt-Väisälä frequency, refer to Fig. 2, using data from CTD⁵ stations which were performed at the deployment and recovery of the instruments. The upper thermocline ranges to a depth of about 350 m and we have plotted the region below this region separately. Interestingly we see a peak at -1000 m, but unfortunately we do not have ADCP records at this depth. We will investigate the influence of stratification on wave propagation in §3.5.

³Postdoc at NIOZ, schout@nioz.nl

⁴ N has been calculated using the SEAWATER toolkit for MATLAB which is based on a modified form of the international equation of state of seawater [10].

⁵CTD: Conductivity, Temperature and Depth.

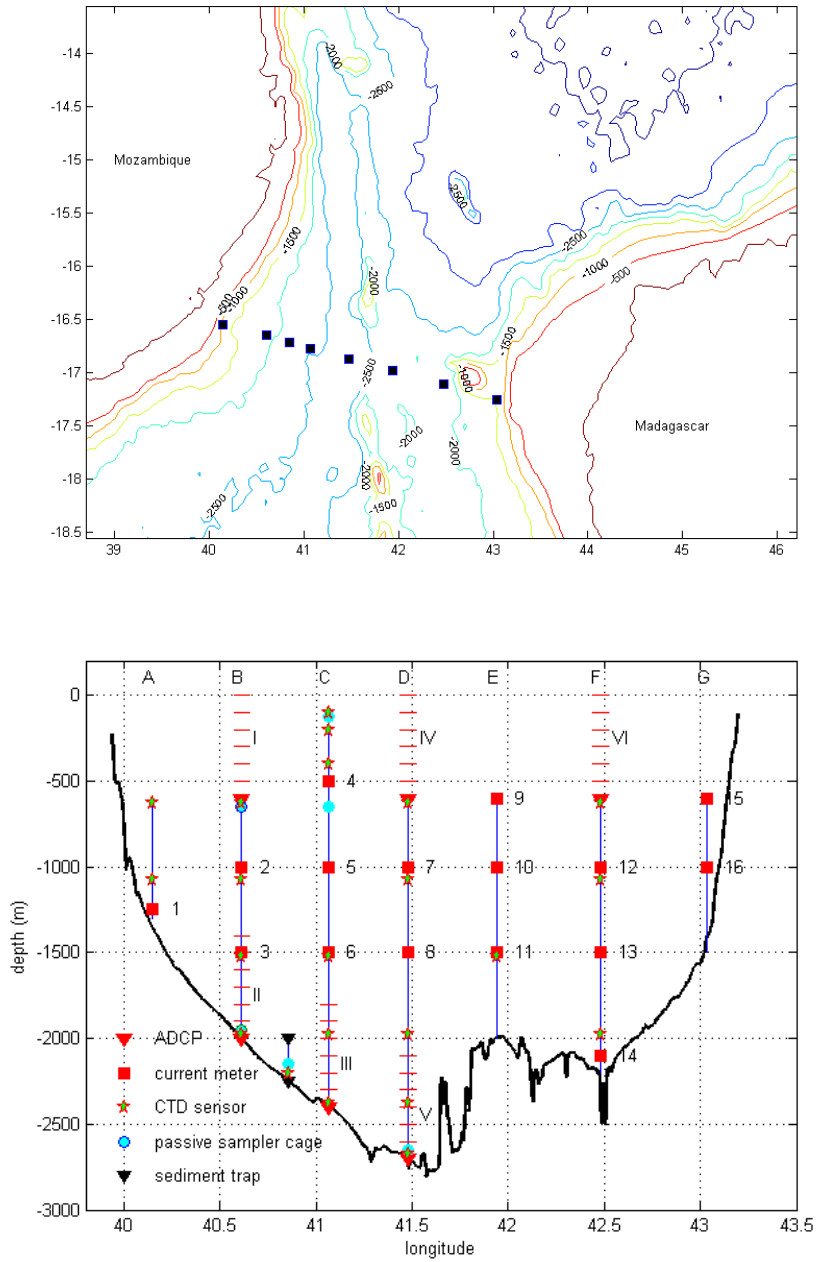


Figure 1: Topography of Mozambique channel. Top: bathymetric chart. Black squares indicate the locations of the moorings. Bottom: cross-channel distribution of instruments. Capitals A-G identify moorings. Numbers 1-16 and I-VI identify current meters and ADCP's respectively. Horizontal lines indicate the range of the ADCP.

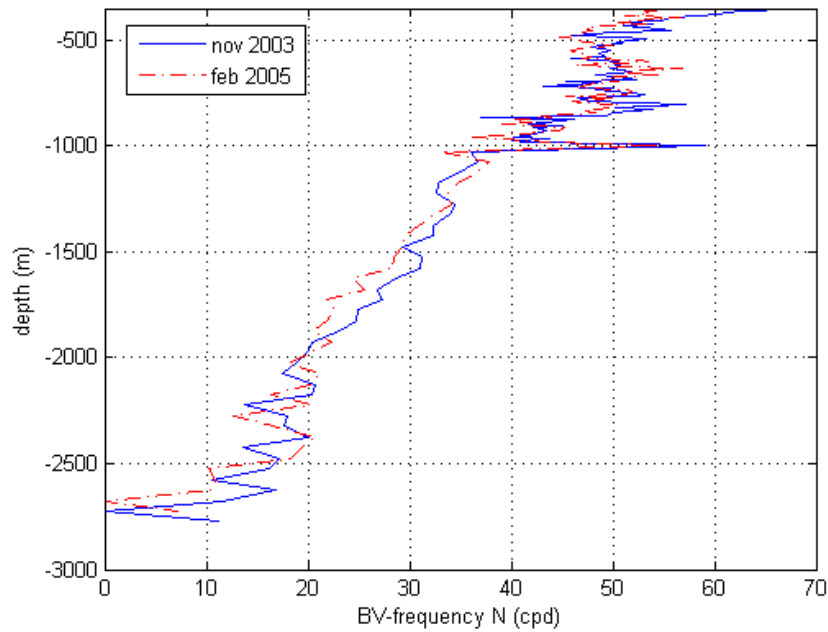
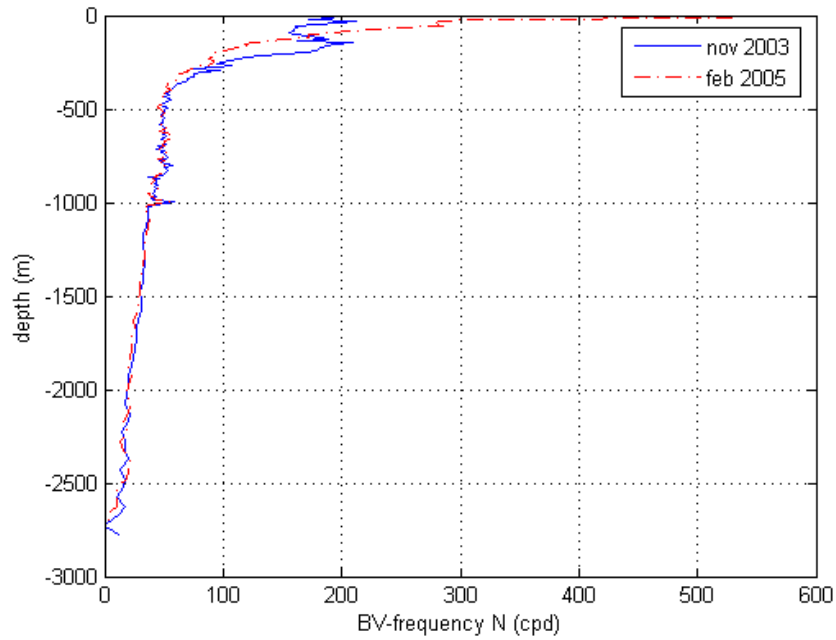


Figure 2: Brunt-Väisälä frequency obtained from CTD stations at deployment and recovery. Top: Complete Brunt-Väisälä frequency profile. Bottom: Same profile under thermocline (in the range from -350 m to bottom). It is remarkable that we see $N = 0$ near the bottom both in the 2003 and the 2005 data.

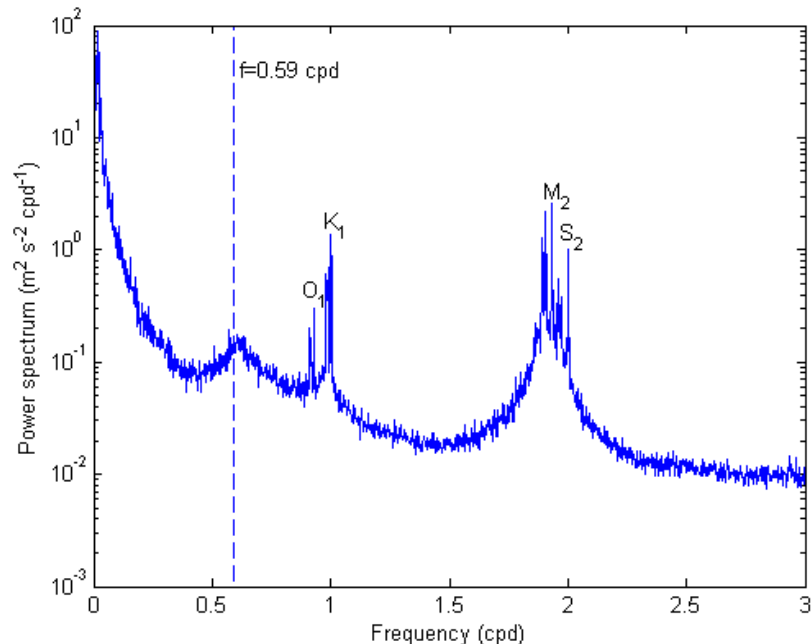


Figure 3: Mean power spectrum of the horizontal velocity obtained by averaging spectra of all ADCP bins and current meters. The local inertial frequency f and the principal tidal constituents are indicated in the spectrum. General note: high energies at low frequencies ($\ll f$) are probably due large scale currents trough the channel.

Most internal waves are driven by gravitational pull from celestial bodies, like the Moon and the Sun. These waves are called internal tides. The main frequencies of internal tides are integer multiples of one day, or more specifically, the time our planet needs to make one revolution (refer to Tab. 3). Apart from gravity there is another restoring force for internal waves, which is even more directly related to the rotation of Earth. This (pseudo-)force is the Coriolis force and it supports so-called internal ‘inertial waves’. In Fig. 3 we see that the semidiurnal wave band is most energetic in the entire mooring period. However, in some periods, the peak-energy of the inertial band is of the same order of magnitudes as the M_2 tidal peak, as can be seen in Fig. 4.

By definition internal waves are baroclinic phenomena. Literally ‘baroclinic’⁶ means that pressure⁷ varies in space, which must be the case for any local perturbation in the ocean, internal waves included. On the contrary, we also distinguish barotropic waves, which are assumed to exist uniformly over the

⁶Latin *clinare*: to lean, slope.

⁷Actually we refer to local pressure minus hydrostatic pressure.

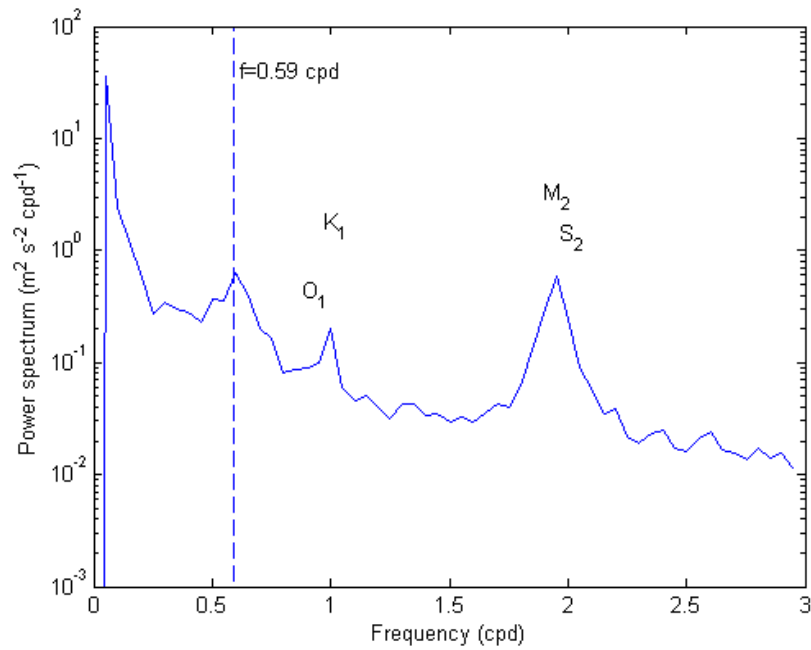


Figure 4: Mean power spectrum of the horizontal velocity in the period from day 115-135, obtained by averaging spectra of all ADCP bins and current meters. Clearly, there is more energy in the frequency band around f compared to the powerspectrum of the entire mooring period, refer to Fig. 3. Actually, the order of magnitude of the inertial peak is comparable to the semidiurnal lunar tide M_2 . Note that the frequency resolution is much lower (0.05 cpd) because we are looking at a 20 day time window.

entire depth range of the ocean. In Figs. 5 and 6 we have plotted the baroclinic powerspectrum at about -500 m and -1500 m depth at mooring site B. We have calculated the barotropic signal by averaging the current of all current meters of the mooring. The baroclinic signal is obtained by subtracting the barotropic signal from the signal of an individual current meter.

3 Near-inertial waves

3.1 Introduction

Pure inertial oscillations owe their existence to the rotation of the Earth. Moving water packets in an unstratified ocean are deflected by Coriolis force and will tend to circular motion, like a free particle on a rotating disk [11]. The orbital frequency on a rotating sphere is given by the inertial frequency f . The motion of inertial oscillations is governed by Coriolis force and pressure gradient [6],

$$\rho_*[\partial_t + 2\vec{\Omega} \times] \vec{u} = -\vec{\nabla} p, \quad (2)$$

where ρ_* is average density, p is pressure and we have assumed an unstratified fluid ($N = 0$). Pure inertial waves are also called ‘gyroscopic waves’ and they can be generated in a homogeneous, rotating fluid. Maas and Manders have observed gyroscopic wave attractors in a rotating rectangular basin with one sloping boundary [12] [4].

In the more realistic, stratified ocean a water packet will float on more dense water. We may take this into account by adding a buoyancy term, $\vec{g}\rho_0$, to (2), where g is the gravitational acceleration. The restoring gravitational force works in the vertical, so we expect an oscillation in this direction as well. For the vertical velocity w we have the equation, $\rho_t - (\rho_* N^2/g)w = 0$ [6]. Hence we see that buoyancy ($N \neq 0$) gives rise to gravitational waves, $\vec{u} = \vec{U} \exp[i(\vec{k} \cdot \vec{x} - \sigma t)]$, which are most abundant in the ocean. Close to f , however, gravity waves are strongly modified by Coriolis force, imposing a horizontal oscillation to the waves. The frequency of gravito-inertial waves is within the so-called ‘near-inertial’ waveband.

Spectral analysis reveals two periods with increased near-inertial wave activity. We have computed a 20 day integrated spectral power profile for the entire mooring period (App. B). Most near-inertial wave energy is concentrated in the period from day 115-135 and 410-430, where we count days from November 17, 2003. In the remainder of this section we will look in detail at the near-inertial waves in these time windows.

3.2 Generation

Near-inertial waves can be generated by any, more or less ‘instantaneous’, disturbance of the sea, both at the surface and in the interior. Actually, there is no particular generation source, in contrast to internal tides, which are continuously generated by the barotropic tide flowing over topographic features. We

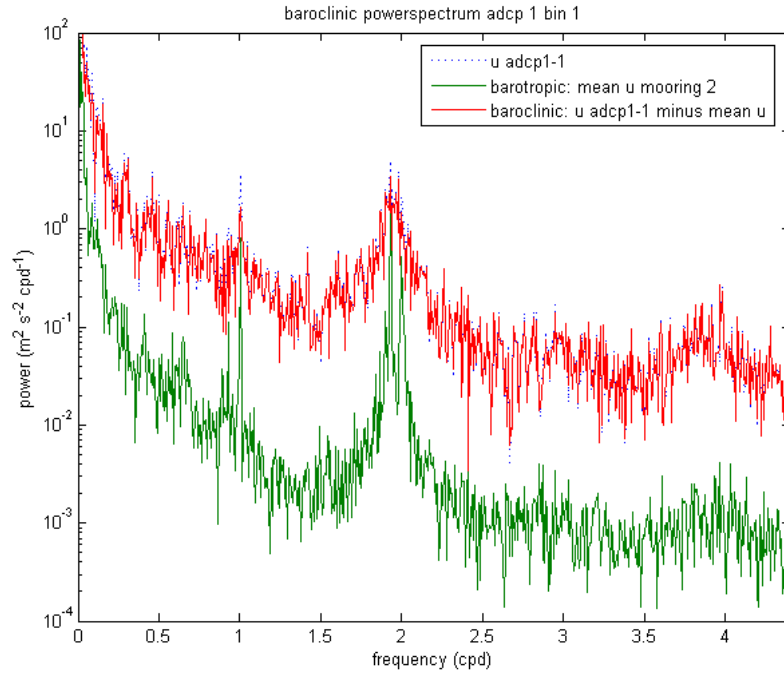


Figure 5: Combined powerspectra of individual current meters, the barotropic signal of mooring B (lower signal) and the baroclinic signal at the first bin of ADCP1 (at about -500 m). We consider the mean of all current meters at the mooring to be the barotropic signal. The baroclinic signal at some point is defined as the individual signal at that point minus the barotropic signal of the entire mooring. In this plot we look at the lowest bin of ADCP1. Except for tidal frequencies we see that the barotropic energy is small compared to the energy at the point of measurement. Therefore, we see an almost perfect overlap of the individual and the baroclinic powerspectrum. Note: all spectra in this figure have been smoothed by dividing the time series in three equal parts and taking the average powerspectrum of the three spectra obtained from these series.

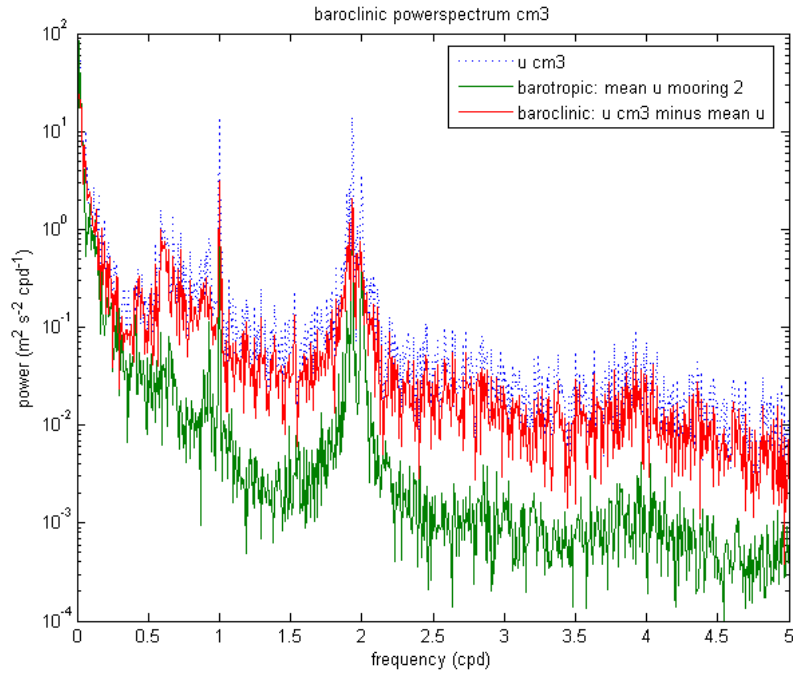


Figure 6: Combined powerspectra of current meter 3, the signal measured by CM3, the barotropic signal of the entire mooring and the baroclinic signal at the current meter. Compared to the lowest bin of ADCP1 in Fig. 5 we see more barotropic energy at all non-tidal frequencies. This means that the baroclinic energy at this depth is lower compared to bin 1 of ADCP1 which is located about 1000 m higher. Note: all spectra in this figure have been smoothed by dividing the time series in three equal parts and taking the average powerspectrum of the three spectra obtained from these series.

Id	Year	Month	Name	Dates	Days
c1	2003	Dec	Cela	9-10	22-23
c2	2004	Jan	Elita	28-31	72-75
		Feb	,,	1-5	76-80
c3		Mar	Gafilo	2-7	106-111
c4	2005	Jan	Ernest	20-23	430-433

Table 1: Tropical cyclones passing Madagascar (source: <http://www.ncdc.noaa.gov/>). Refer to App. 4 for cyclone tracks and an brief description.

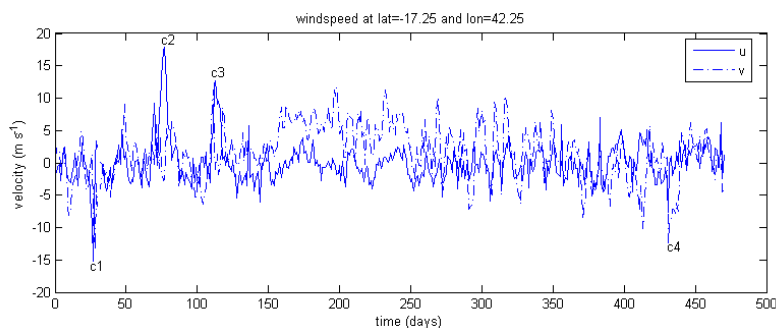


Figure 7: Windspeeds in u and v direction at 17.25°S and 42.25°E . Measurements were made by QuikSCAT, a scatterometer satellite.

have been looking at tropical cyclones and eddies to see whether these events could have generated inertial waves. In fact, it seems likely that most inertial waves are caused by cyclones. In Tab. 1 we have listed all official cyclones that have passed the channel during the measurements.

Cyclone ‘Gafilo’ preceded the intense inertial wave activity in the first period (day 115-135). ‘Ernest’ struck the island in January 2005 coinciding with the second period of inertial wave activity. Tab. 1 shows that Madagascar is tormented by cyclones on a regular basis. The sea surface has been stirred by three cyclones in the first four months after deployment. ‘Cela’ was a pretty modest storm and we see little effect in the sea current. ‘Elita’ wandered around in the area for quite some time. During passage of Elita we see many inertial oscillations close to the Mozambique shelf (compare ADCP1 and ADCP6 in App. D). In Fig. 7 we have plotted satellite records of wind speeds at the centre of the mooring cross-section.

Finding specific events that have generated inertial wave packets is not always possible. The filtered ADCP data in App. D shows there is inertial wave activity at almost all times. Fig. 8 gives an overview of the inertial waves measured by the ADCP’s, together with tropical cyclones, eddies and the 2004 Indian ocean tsunami. Looking at this picture it is tempting to relate inertial

waves to cyclones, but we could not find an generative event for all inertial wave packets.

3.3 Interaction with eddies

Eddies are large current vortices in the ocean. These large (hundreds of kilometres diameter), rotating water masses affect the local inertial frequency, $f = f_{Earth} + f_{eddy}$. Close to the Mozambique channel they split off from the Indian ocean circulation on a regular basis. Preceding observations in the Mozambique channel did not reveal interactions between eddies and internal tides [13], but we expect the interaction effects to be much larger in the near-inertial waveband.

Assuming an eddy diameter comparable to the width of the channel, we have identified three large eddies by looking at the relative current at the east and west side of the channel. In Fig. 9 we compare the average velocity in the meridional direction as measured by ADCP1 with the same velocity component measured by ADCP6. As expected, we see that most water flows to the south, along with the background current through the channel. However, at the Mozambique side of the channel, the current flows northward regularly and at considerable high speed. This is probably due to eddies, which rotate in counter-clockwise direction at the southern hemisphere.

The eddy vorticity may be derived from Fig. 9 and Fig. 1. The figure with the moorings shows that ADCP1 and ADCP6 are about two longitudinal degrees apart at about 17°S, in kilometres this distance would be about 212 km. We assume solid body rotation and use the definition of vorticity $f \equiv v_x - u_y = \Delta v / \Delta x - \Delta u / \Delta y$. For simplicity we take $\Delta u = -\Delta v = -1$ m/s and with $R = \Delta x = \Delta y = 106$ km we obtain $f_{eddy} = 2/R = 1.89 \cdot 10^{-5}$ rad s⁻¹ = 0.26 cpd, which is about 40% of the local vorticity due to the rotation of the Earth.

Since eddy and Earth rotate in opposite directions we will have to account for an intermittently lowered inertial frequency. We would expect more energy at frequencies smaller than $f_{Earth} = 0.59$ cpd in the presence of an eddy. To demonstrate this effect we have chosen 8 current meters in the centre of the channel, which we expect to be well within the eddy vortex. In Fig. 10 we compare the powerspectra of periods with and without eddy for each current meter.

The picture we obtain from Fig. 10 is suggestive but not conclusive. The sub-inertial energy differs from current meter to current meter and we do not see consistent higher energies in the presence of eddies. However, we do see that sub-inertial energy dominates in the presence of eddies at current meters 4, 7 and 9. This is interesting because these current meters are closer to the surface and more to the middle of the channel, right where we expect maximal eddy vorticity.

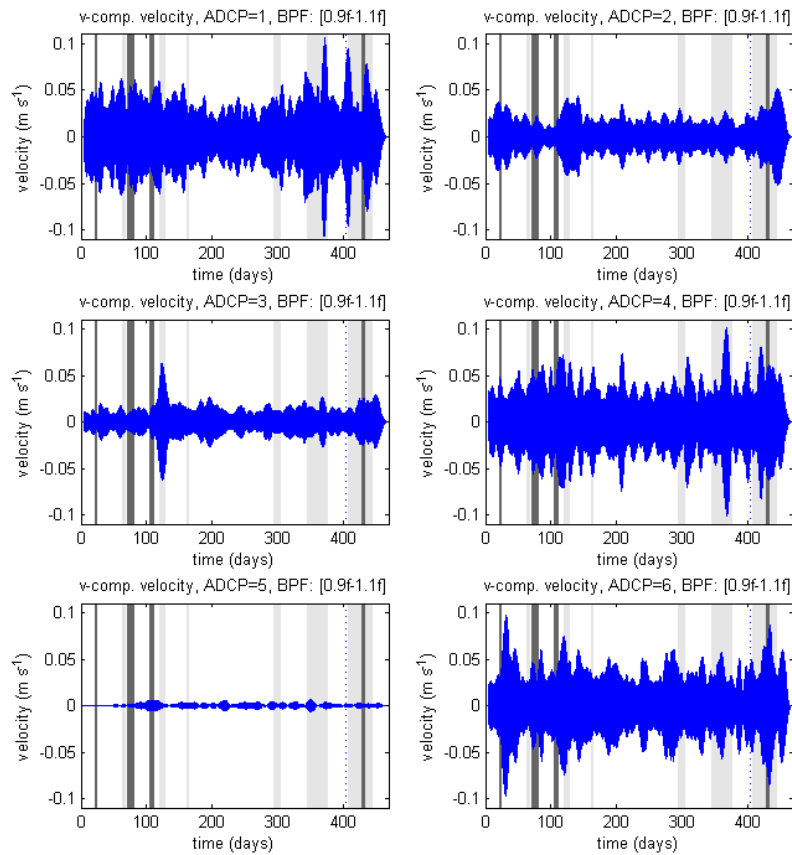


Figure 8: Possible generation sources for inertial waves. ADCP signals have been bandpassfiltered between $0.9f$ and $1.1f$ and all bins are displayed on top of each other. Dark shaded areas indicate the presence of a tropical cyclone. Light shaded time windows coincide with the passage of a large eddy. The dotted line is plotted at UTC 10.00 Dec 26, 2004, which is approximately the moment when the Sumatra-Andaman tsunami arrived at the mooring transect. Although cyclones do not occur from Apr until Dec 2003, we do see strong winds in this period, especially from day 160-320, as is shown in Fig. 7.

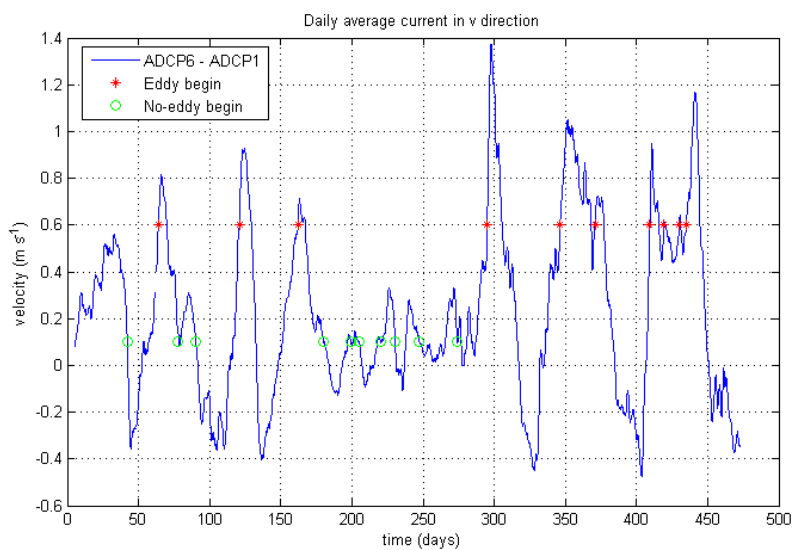


Figure 9: Eddy signal. We use the daily average meridional current velocity of ADCP1 at the Mozambique side and ADCP6 at the other side and take the difference: $ADCP6 - ADCP1$. Assuming an eddy diameter comparable to the width of the channel we may regard this signal as an indication for the presence of an eddy. We assume eddy presence if $ADCP6 - ADCP1 > 0.6 \text{ m s}^{-1}$ and eddy absence if $ADCP6 - ADCP1 < 0.1 \text{ m s}^{-1}$.

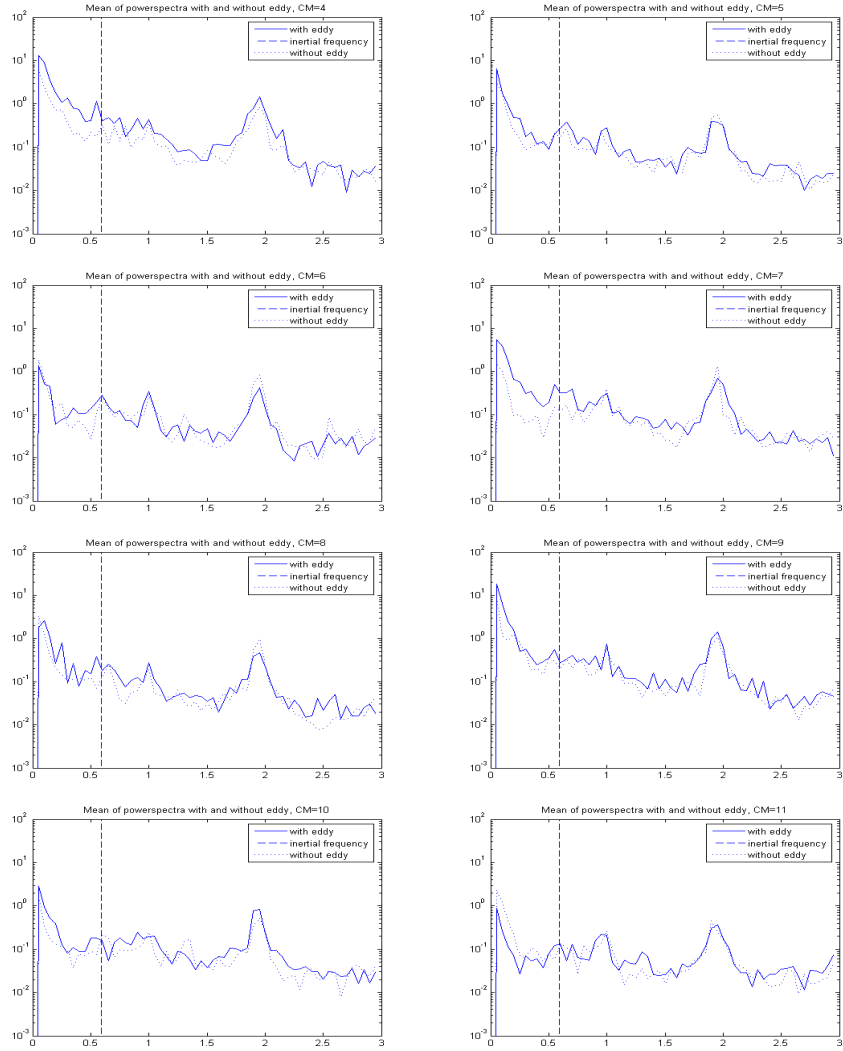


Figure 10: Powerspectra of 20 day periods with and without eddy. current meters 4, 7 and 9 are supposed to be in the centre of the eddy. Note that the indicated inertial frequency refers to the vorticity due to the rotation of the Earth (f_{Earth}).

3.4 Energy and phase

Internal waves are dispersive, which means that the propagation speed depends on the wave vector $\vec{k} = (0, k, m)$. From the dispersion relation,

$$\sigma^2 = N^2 \cos^2 \theta + f^2 \sin^2 \theta, \quad \text{with } \vec{k} = |\vec{k}|(0, \cos \theta, \sin \theta), \quad (3)$$

follows that phase (along \vec{k}) and energy (along $\vec{c}_g = (0, \frac{\partial \sigma}{\partial k}, \frac{\partial \sigma}{\partial m})$) propagate in perpendicular directions, $\vec{c}_g \perp \vec{k}$ [7]. For $N > f$ we find that the direction of horizontal propagation of group velocity and wave vector is equal, whereas vertical components propagate in opposite directions.

3.5 Propagation

Interpreting the spatial behaviour of internal waves poses quite a challenge, since the length scale of the wave is typically small compared to the spatial resolution of the measurements. We have current records of 122 locations in a $\sim 500 \text{ km}^2$ cross-section of the Mozambique channel. In the along channel direction we only have information in a single plane. Cross-channel we have 7 moorings, about 35 km apart. ADCP's provide high resolution in the vertical (25 m), but only 6 of these instruments have been deployed.

The ADCP measurements allow us to estimate the vertical component of the group velocity. Based on Fig. 11 we find $v_g = -1.16 \pm 0.17 \text{ mm/s}$ for the vertical group velocity. This velocity is low, but we have to keep in mind that inertial waves propagate almost horizontally. Using this value for the vertical group velocity we have calculated the wavelength $\lambda = 2\pi/|\vec{k}|$ and the horizontal group velocity $\partial\sigma/\partial k$. Because Eq. 3 does not work at $\sigma = f^8$ we have used the non-traditional dispersion relation [14],

$$\sigma^2 = N^2 \cos^2 \theta + (f_s \cos \theta + f \sin \theta)^2, \quad (4)$$

with $\vec{f} = (0, \tilde{f}, f)$, $f_s = \tilde{f} \sin \alpha$, and $(\cos \alpha, \sin \alpha)$ the direction of wave energy propagation. For wave propagation along the mooring transect and with $N = 1.45 \cdot 10^{-2} \text{ rad s}^{-1}$, we obtain $\lambda = -415 \text{ km}$ and $\partial\sigma/\partial k = 20.7 \text{ m s}^{-1}$.

At first these values for wavelength and horizontal group velocity seemed very high to us. We looked at the input parameters to see where these extreme values come from. However, tuning the vertical velocity does not help a lot, since $\lambda, \partial\sigma/\partial k \propto \partial\sigma/\partial m$ and we estimated the error to be at most 15%. Other parameters are quite well known, except for the buoyancy frequency (N), which varies at least 300% in the upper 500 meters and moreover $\lambda, \partial\sigma/\partial k \propto N^2$. Taking N four times smaller we obtain wavelengths that would at least fit into the channel (refer to Tab. 2). Later we discovered that our initial findings are not exorbitant and in accordance with literature values. Qi et al. [15] found 140-410 km for the horizontal wavelength and 150-1500 m for the vertical wavelength.

⁸The traditional relation gives $k = 0$ at $\sigma = f$.

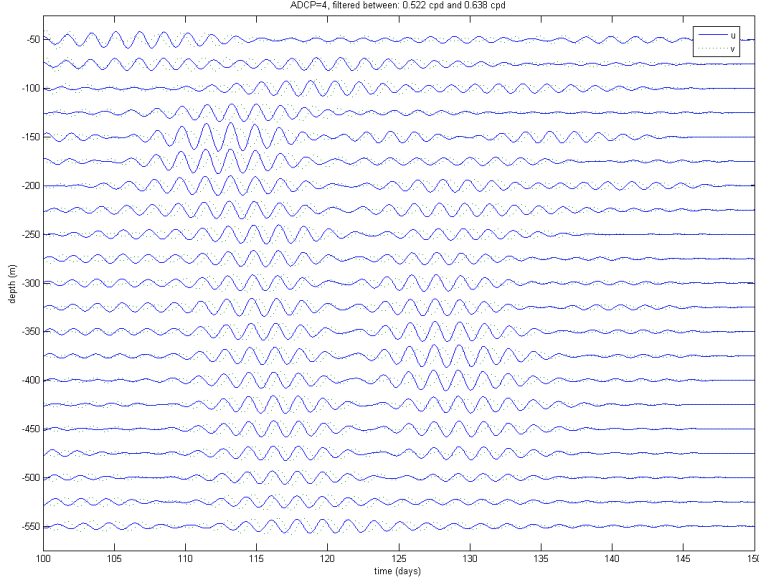


Figure 11: Current velocity measured by ADCP4. The signal is bandpass filtered between $0.9f$ and $1.1f$. From this plot we derived a vertical group velocity of 100 ± 15 m per day.

N (cpd)	λ (km)	$2\pi/k$ (m)	$\partial\sigma/\partial k$ (m s^{-1})
along mooring transect ($\alpha = 15^\circ$)			
200	-415	23.2	20.7
50	-26.0	23.2	1.30
perpendicular to mooring transect ($\alpha = 105^\circ$)			
200	-934	52.2	20.7
50	-58.4	52.2	1.30

Table 2: Wavelength (λ), vertical wavelength ($2\pi/k$) and horizontal group velocity ($\partial\sigma/\partial k$), calculated using Eq. (4) with $\partial\sigma/\partial m = -1.16 \cdot 10^{-3} \text{ m s}^{-1}$. These results deserve further attention, because it is strange that we got a minus sign in front of the wavelength and that the vertical wavelength does not significantly change for different N .

Based on App. D we have formulated a preliminary interpretation of inertial wave propagation in the period from day 115-135.

1. Wave is generated at ADCP4 around day 105.
2. In ~ 8 days it travels downward to -125 m.
3. In ~ 6 days it propagates from -125 m to -600 m.
4. At day 121 it arrives at ADCP3.
5. In ~ 2 days it travels down to the bottom, where it reflects (?) and travels up in ~ 12 days. Close to the bottom the wave seems to have split up.
6. At day 137, when the reflected wave leaves ADCP3, we see a wave packet half-way ADCP2, travelling in upward direction.
7. Around day 150 we see a wave-packet passes the upper six bins of ADCP1.

In App. E we have produced u versus v hodographs. According to traditional theory we expect inertial waves to be circularly polarized. The hodographs, however, show strong ellipticity at several depths. Non-circular inertial waves have been observed before, for example in the Mediterranean Sea [16]. The rectilinear motion in the Mediterranean occurred in regions of extremely low stratification and could therefore be explained by non-traditional β -plane effects [17]. These effects come into play at a typical buoyancy of $N = 7$ cpd. The buoyancy frequency in the Mozambique channel is of this order of magnitude close to the bottom (Fig. 2). But, remarkably, we also see non-circular hodographs at greater heights and even close to the surface.

ADCP's also provide information on the vertical displacement of water. At first we have discarded the vertical velocity in our analysis, but in App. F we include some crude data. Powerspectra of the vertical velocity show the tides very nicely (App. F.2). Kinetic energy around the inertial frequency is low for vertical currents, as one would expect, because inertial waves oscillate in an almost perfectly horizontal plane.

4 Reflection at boundaries

The dispersion relation of internal waves (Eq. 3) is somewhat peculiar, since frequency does not depend on the magnitude of the wave vector, but on its direction only. This implies that every frequency has its proper angle of propagation, like light propagating through a prism. The angle of the wave vector with respect to the horizontal is given by,

$$\tan^2 \theta(z) = \frac{N^2(z) - \sigma^2}{\sigma^2 - f^2}, \quad (5)$$

where N is the Brunt-Väisälä frequency, σ is wave frequency and f is the inertial frequency.

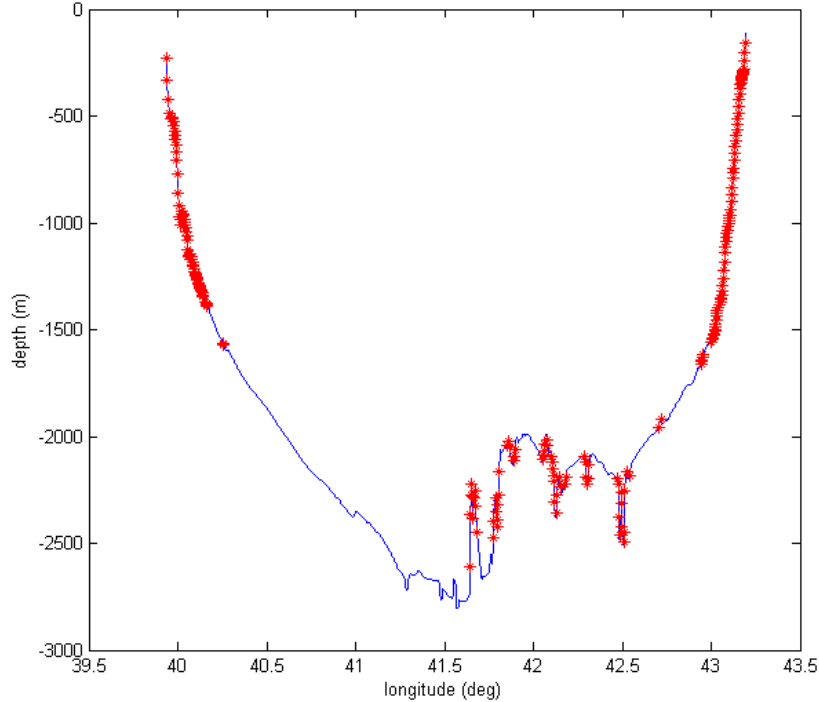


Figure 12: Critical slopes indicated with asterixes for internal wave frequency $\sigma = M_2$, $f = 0.59$ cpd and de Brunt-Väisälä frequency is the average of Nov 2003 and Mar 2005 as given in Fig. 12.

An internal wave reflecting on a slope maintains its angle of propagation. A beam of parallel wave rays will therefore (de)focus on a sloping boundary [1]. Wave energy focusses at steep slopes. A slope is called supercritical if its steepness-angle (α) is larger than the propagation angle of the wave. In terms of Eq. 5 it must obey, $\alpha > \pi/2 - \theta$. In Fig. 12 we have indicated critical slopes for the principal lunar tide.

5 Discussion

This research focusses on internal inertial wave analysis of recent measurements in the Mozambique channel. We will discuss generation of this kind of waves, interaction with eddies and propagation. For further analysis and discussion we have attached figures and tables in the appendix.

Internal inertial waves are thought to be mainly wind generated. In a few cases we could indeed relate inertial wave packets to extreme weather events.

Based on spectral power analysis we identified two periods of high energetic internal waves. These periods were both preceded by the passage of a tropical cyclone, so we may assume that those winds have generated the inertial waves. Other periods of increased inertial wave activity could not be related to specific winds.

We have also been looking at the interaction of eddies with inertial waves. We found that the local inertial frequency can be significantly lowered by the vorticity of an eddy. This means that inertial waves can oscillate at lower frequencies during the passage of an eddy. To see whether these lower frequencies do exist we have compared powerspectra of periods with and without eddy. Our results are not unambiguous, but we do see increased sub-inertial energy for current meters close to the centre of the passing eddy.

Propagation of internal waves in the ocean is a tricky subject. We do not know how and where these waves are generated, we do not know in what direction they will propagate, we do not know the wavelength and even the conditions of the supporting medium and its boundaries are largely unknown. We know almost nothing and to learn more we only have a small shipload of instruments to measure current velocities.

In our analysis we did not manage to see clear wave beams, although we extensively looked at several graphical layouts of the data. For this reason and because of limited time available we did not look at wave propagation in a more quantitative manner. It would be interesting to calculate correlations of amplitudes and phases as a function of time and see whether periods exist where a wave beam passes along two or more current meters.

Obviously, the configuration of instruments was not designed for detection internal inertial waves. In fact it was intended for measuring large scale water transport through the channel and therefore only a cross-channel transect was deployed. For detection of internal waves we would prefer a 3D distribution of instruments. We would need a relatively high spatial resolution, if we want to detect waves directly.

The question regarding the ellipticity of the hodographs remains open. We have observed hodographs showing strong ellipticity at many depths, both close to the bottom and just below the surface. Whereas, theoretically, we would expect circularly polarized hodographs.

Vertical velocity measurements have only been analysed superficially. These velocities are considered rather insignificant regarding inertial waves, but they are interesting with regard to internal tides.

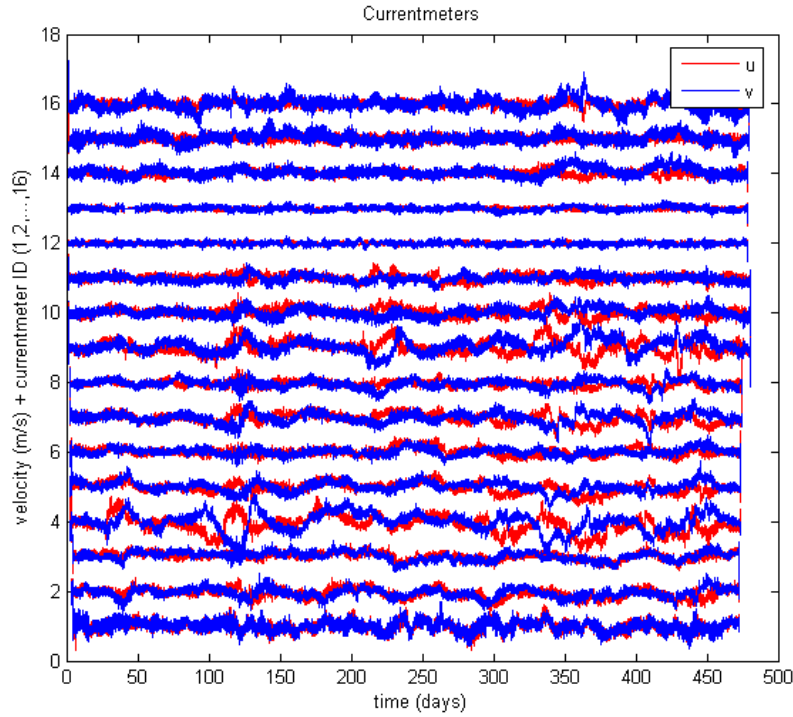
As a matter of fact we have disregarded internal tides almost completely. Again, the main reason for this is that we ran out of time and moreover internal tides in the Mozambique channel have already been studied by Manders et al. [4].

As a concluding remark, I would like to say I have enjoyed doing this research. I also believe that we reached many of the objectives, although we did not find a wave attractor, which could be considered the holy grail of this field. Anyway, I learned a lot about physical oceanography and I definitely experienced doing research myself.

Acknowledgements I realize that this ‘post-graduation’ internship is somewhat beyond regular course and therefore I really appreciate the hospitality of the Royal NIOZ. Many thanks also to the people of the physical department. In the first place I want to thank my mentor, Leo Maas, for gently and very patiently introducing me to the subject. Theo Gerkema has been very helpful for support regarding ‘non-traditional’ theory. I would like to thank Hans van Haren, the realist in the field, for discussions and suggestions. All others, whom I did not mention in person, have been great company during my days at the institute. Thanks.

A Raw data

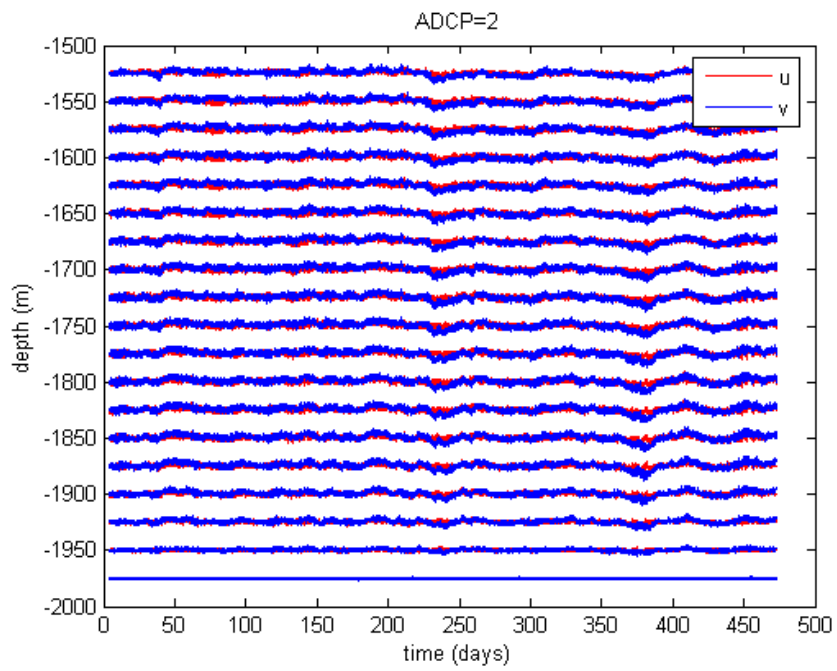
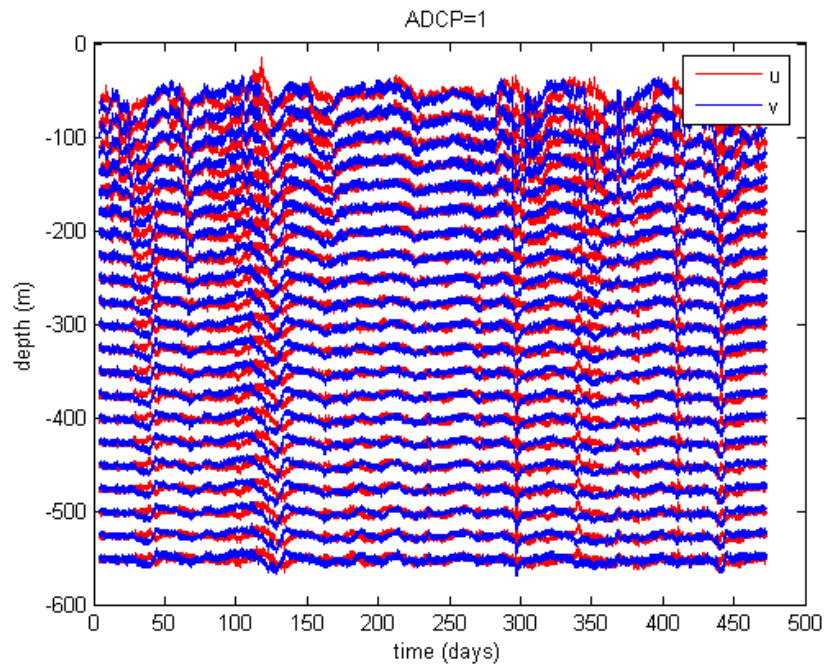
A.1 current meter data

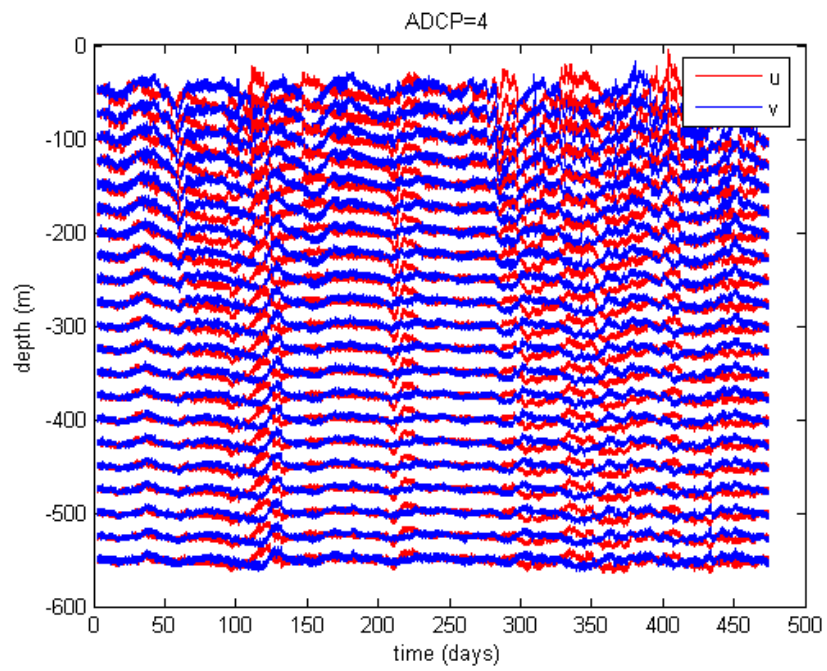
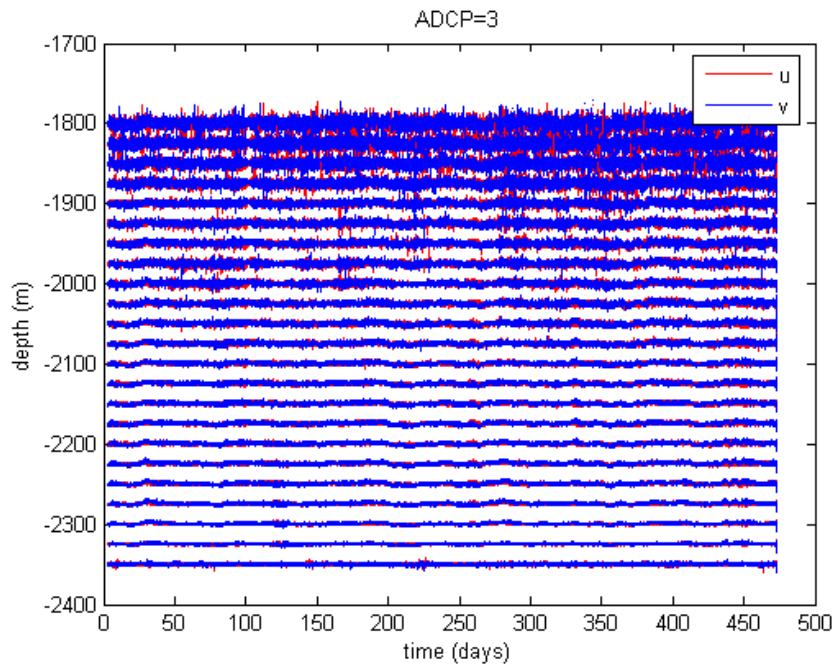


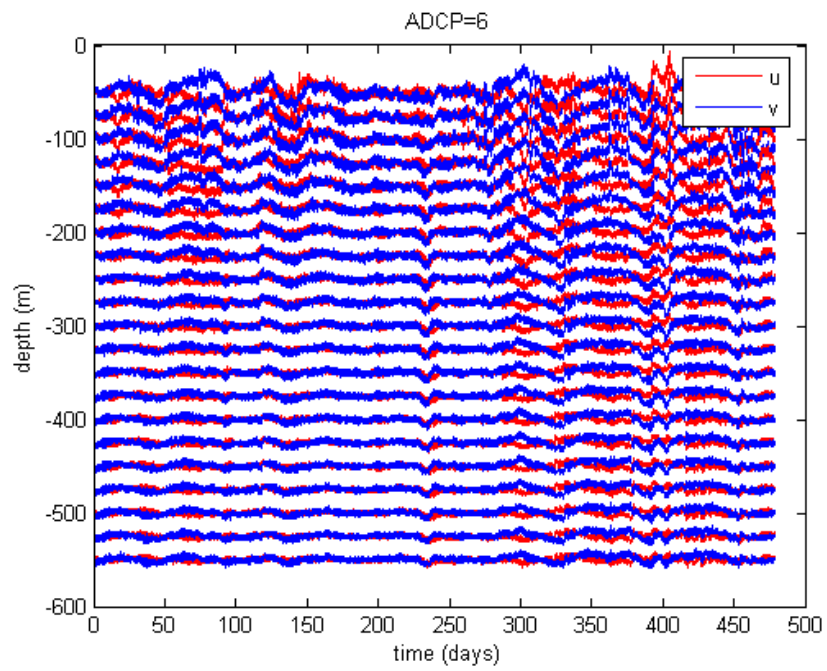
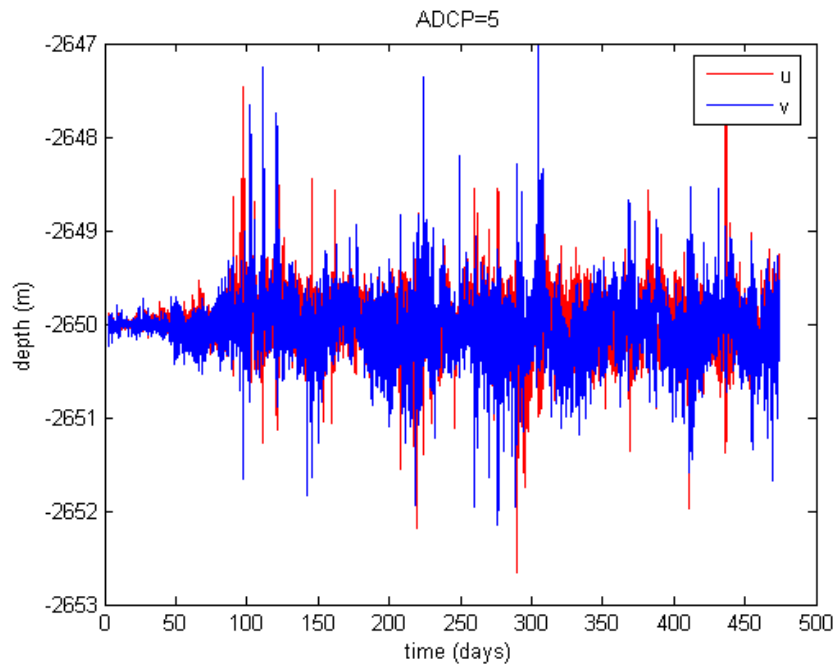
The time series from current meter 12 and 13 looks different from the rest. From [9] we learned that all current meters are of the type RCM11, except for 13 and 14 which are RCM8. The average amplitude of 13 and 14 is about 2.5 times smaller than the surrounding current meters and the energy in M2 is even a factor > 10 smaller. We will disregard these current meters in our analysis.

A.2 ADCP data

Raw signal from ADCP's. The velocity has been multiplied with a factor 25 and is in m/s.

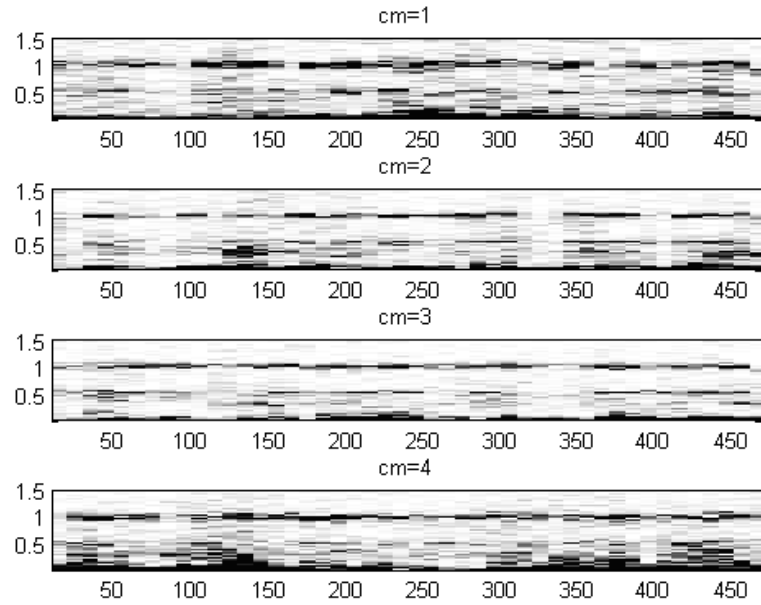


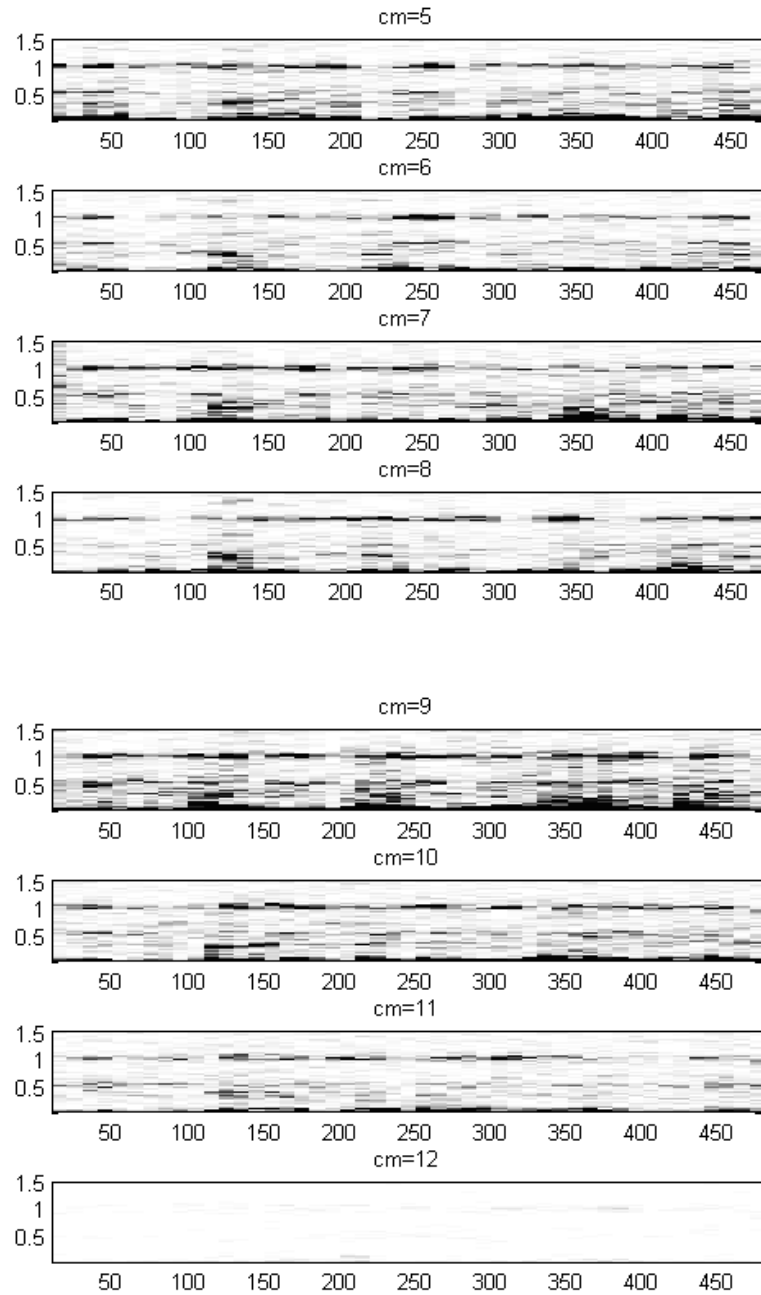


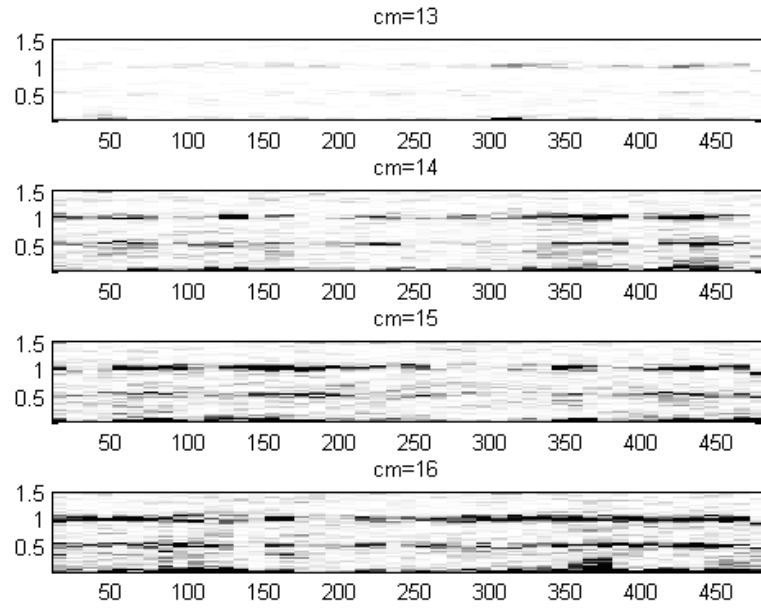


B Slided powerspectra

We have computed the spectral power in a 20 day time window and we have slided this window through the entire time domain with an overlap of 10 days. Energy is indicated in greyscale, where black is most energetic. Frequency in cpd is along the vertical axis.







C ADCP phases and energies at inertial frequency

We calculated individual phases (in radians) and energies (in $\text{m}^2 \text{s}^{-2}$) in the period 115-135 for $\sigma = f$. Energies are summed over $i_f - 1$ and $i_f + 1$, with i_f the index of the inertial frequency. From left to right columns represent $\phi_u, \phi_v, \phi_v - \phi_u, E_u$ and E_v . Note: With data from ADCP3 we had problems calculating phase and energy in the higher bins.

adcp =

1

ans =

-0.0543	3.0673	3.1216	2.7236	0.6906
-0.8715	0.3917	1.2632	2.5597	0.2648
-0.8582	-0.5263	0.3319	2.1738	0.6640
-0.8881	-1.0572	-0.1691	1.7510	0.3890
-1.2357	-2.4021	-1.1664	1.9183	0.8770
-1.0751	-2.2438	-1.1687	0.9971	1.0988
-1.3882	-2.1178	-0.7295	0.9320	0.8789
-1.9513	2.8093	4.7606	0.8228	0.8384
-2.0504	2.4117	4.4621	0.9682	0.9858
-2.1450	1.8308	3.9758	1.5641	1.2433
-1.9198	2.3367	4.2564	1.8882	0.9094
-1.6247	2.6237	4.2484	2.5146	0.6530
-1.6371	2.5220	4.1591	2.7701	0.6130
-1.5595	-2.7037	-1.1442	2.1495	0.5144
-1.5402	2.6553	4.1954	1.9618	0.5150
-1.4384	-2.1469	-0.7085	1.4245	0.4623
-1.3446	-0.2536	1.0909	1.0023	0.5372
-1.1024	-0.1855	0.9169	0.8100	0.9396
-1.1788	-0.3254	0.8535	0.9111	0.9604
-0.8822	0.0008	0.8830	0.9384	0.9756
-0.6291	0.0260	0.6551	0.7138	0.9192

adcp =

2

ans =

-0.1670	-1.6022	-1.4353	0.2174	0.3131
1.0935	-1.1279	-2.2214	0.2300	0.3509
1.1169	-0.5190	-1.6359	0.3733	0.4046
1.9929	0.1876	-1.8053	0.3695	0.3850
2.3861	1.1121	-1.2740	0.3731	0.4994
2.9854	1.7123	-1.2731	0.4163	0.4497
-2.9787	2.2502	5.2289	0.4781	0.5539
-2.2507	2.5159	4.7666	0.3485	0.4976
-1.8952	2.8256	4.7208	0.2720	0.3847
-1.8716	2.6748	4.5464	0.1424	0.2107
-2.7572	2.5271	5.2843	0.0322	0.1384
2.4407	2.1361	-0.3045	0.0995	0.1430
1.2665	2.8875	1.6210	0.2049	0.2170
1.7382	1.8547	0.1165	0.2451	0.2882
1.6724	2.6290	0.9566	0.2493	0.3337
2.2670	2.5408	0.2738	0.3546	0.3994
2.6779	2.0827	-0.5952	0.3480	0.3970
-3.1287	1.5885	4.7172	0.1951	0.1915
1.9726	2.2850	0.3124	0.0043	0.0027

adcp =

3

ans =

[NB bins containing NaN's and other non-regular numbers have been deleted]

-0.1764	-2.4328	-2.2565	0.4188	0.4369
-0.2102	-2.4980	-2.2878	0.5426	0.7151
-0.2544	-2.4120	-2.1576	0.8582	0.9565
-0.0258	-2.2395	-2.2137	0.9558	0.9837
0.1416	-1.5753	-1.7169	0.6786	0.5992
-0.0633	-1.8492	-1.7858	0.1325	0.1311

adcp =

4

ans =

-1.7329	1.6017	3.3345	2.2010	1.4231
-1.6583	2.2015	3.8598	2.4164	2.2042

-1.2306	2.0351	3.2656	3.1700	1.8115
-1.1262	2.0862	3.2124	1.3638	0.3366
-1.1422	2.4233	3.5655	1.4202	0.8437
-1.1706	-3.0652	-1.8946	2.3636	1.6956
-1.0442	-3.0422	-1.9980	1.8565	1.7991
-0.6069	-2.0529	-1.4461	1.6204	1.8575
-0.0980	-1.2474	-1.1494	1.3322	2.1389
0.0363	-0.6549	-0.6912	1.4034	2.7300
0.1577	-0.2031	-0.3608	1.4196	2.5667
0.7708	-0.4802	-1.2510	1.7364	2.0357
0.9163	-0.3420	-1.2582	1.9787	1.7983
1.1308	-0.1765	-1.3073	2.4655	1.9220
1.3742	0.1868	-1.1875	2.1890	1.4827
1.6248	0.3992	-1.2256	1.9078	1.4764
1.4124	0.6393	-0.7731	1.8038	1.2822
1.5171	0.7607	-0.7564	1.3352	1.0422
2.0244	0.8505	-1.1738	0.8520	1.0622
2.5230	0.8969	-1.6261	0.7747	1.4351
2.6548	0.9588	-1.6960	1.2728	1.2936

adcp =

5

ans =

0.0600	-1.7361	-1.7961	0.0069	0.0034
--------	---------	---------	--------	--------

adcp =

6

ans =

-2.2340	-1.5923	0.6417	1.5935	0.8992
-1.9631	-2.4315	-0.4684	2.0322	1.4489
-1.4500	-2.1054	-0.6554	1.4307	1.1195
-0.7109	-1.5385	-0.8276	1.3264	1.3258
0.0632	-1.0943	-1.1576	1.5725	2.1560
0.6092	-0.3595	-0.9687	1.1676	1.4809
2.5427	1.1908	-1.3519	0.6643	0.9289
-2.9746	2.2384	5.2130	0.6368	0.5322

-2.6506	2.3502	5.0007	0.4569	0.5610
-2.0575	2.4875	4.5450	0.5748	0.5168
-2.0592	2.8896	4.9488	0.5800	0.4638
-1.4092	-2.6267	-1.2176	0.3590	0.3920
-0.4233	-1.2692	-0.8459	0.2252	0.3492
1.1264	0.1917	-0.9347	0.3928	0.3470
1.4788	0.0580	-1.4208	0.3985	0.3463
1.4464	0.5538	-0.8926	0.3376	0.3443
1.8192	0.1895	-1.6297	0.2255	0.2076
-1.7362	-0.5353	1.2009	0.2923	0.1904
-1.2688	-1.8467	-0.5779	0.2862	0.2874
-1.1598	-3.0369	-1.8772	0.3527	0.4931
-2.5913	2.5973	5.1885	0.2874	0.3920

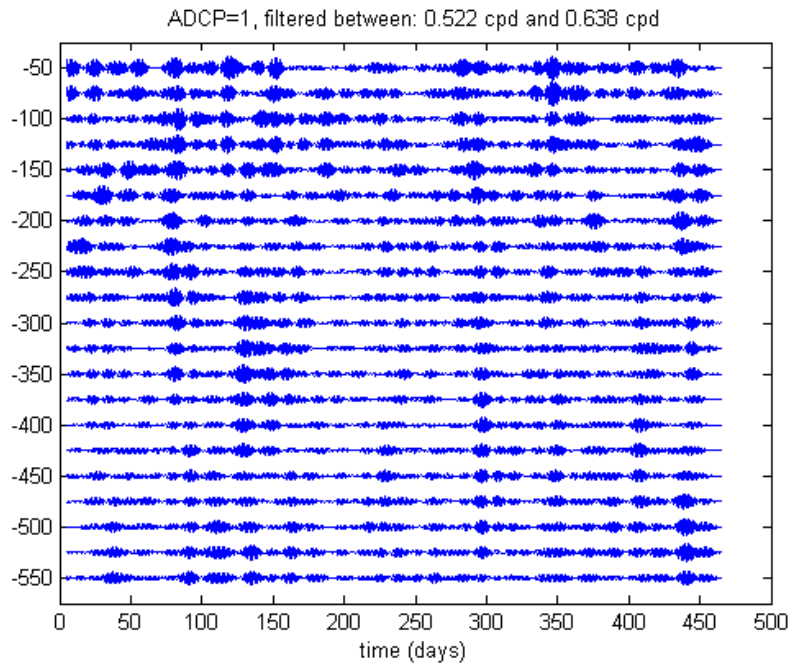
>>

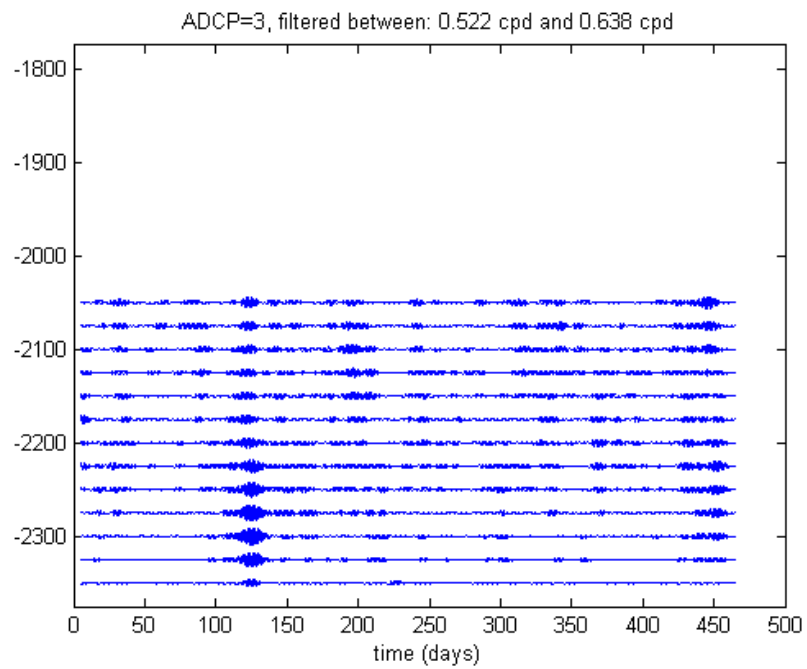
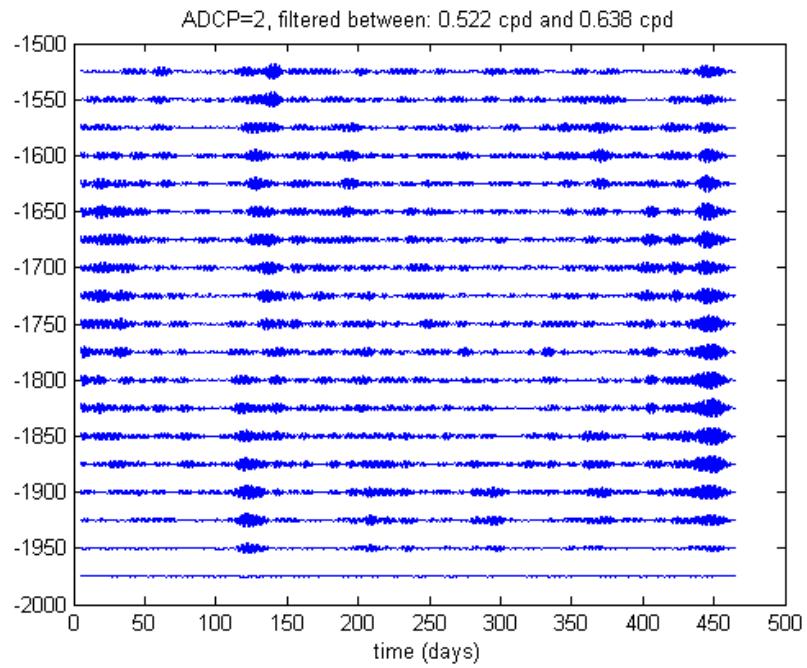
I'D LIKE TO PLOT EQUIPHASE LINES, BUT HOW?

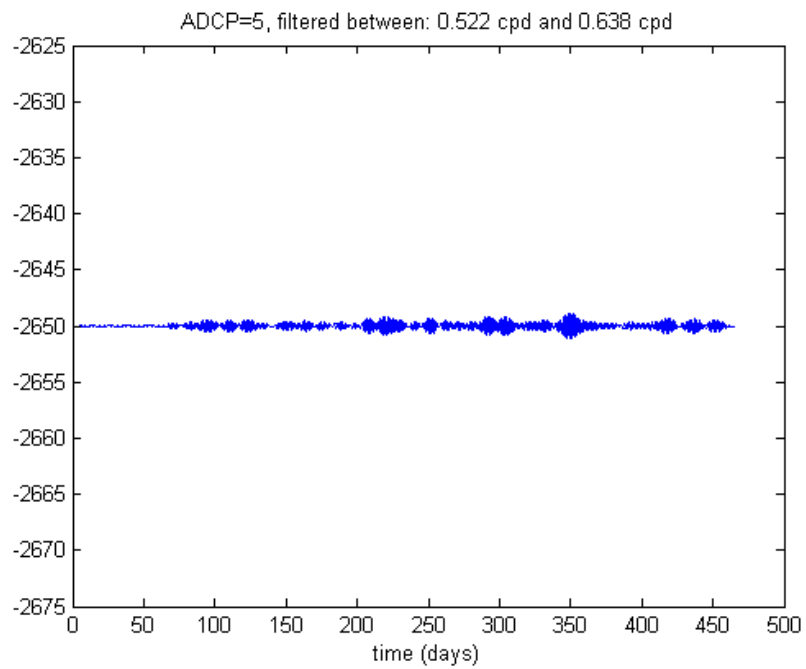
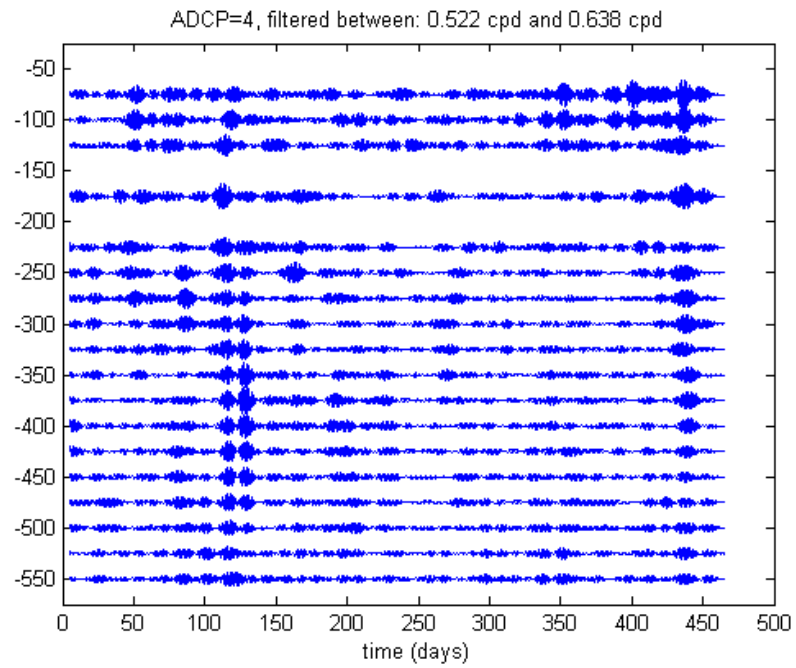
D Filtered data

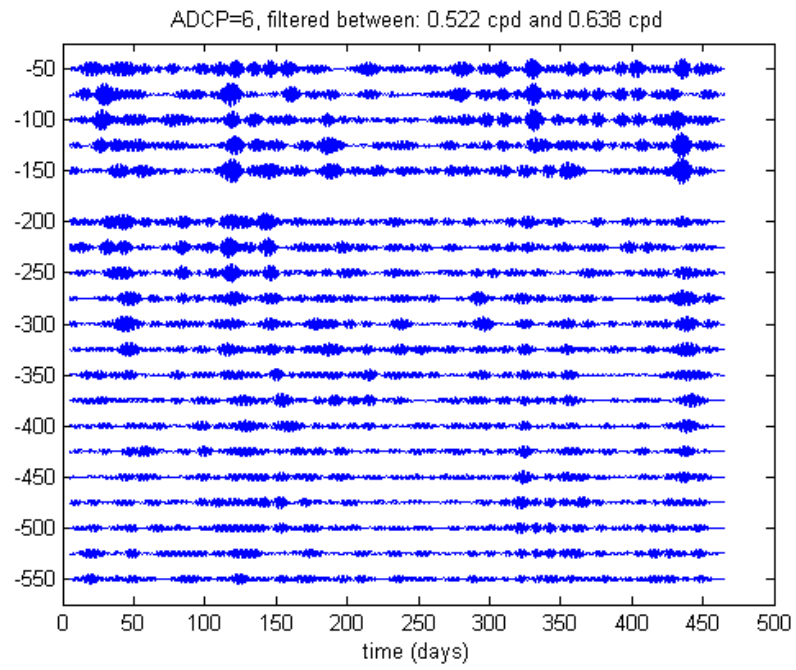
We filtered all ADCP data between $0.9f$ and $1.1f$. NB: velocities have been multiplied by a factor 150.

D.1 Zonal velocity (u)

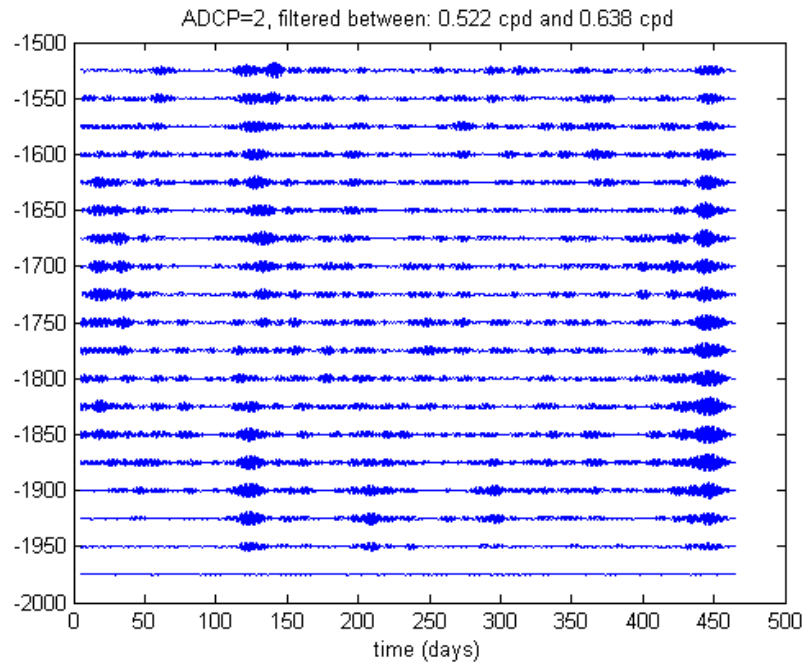
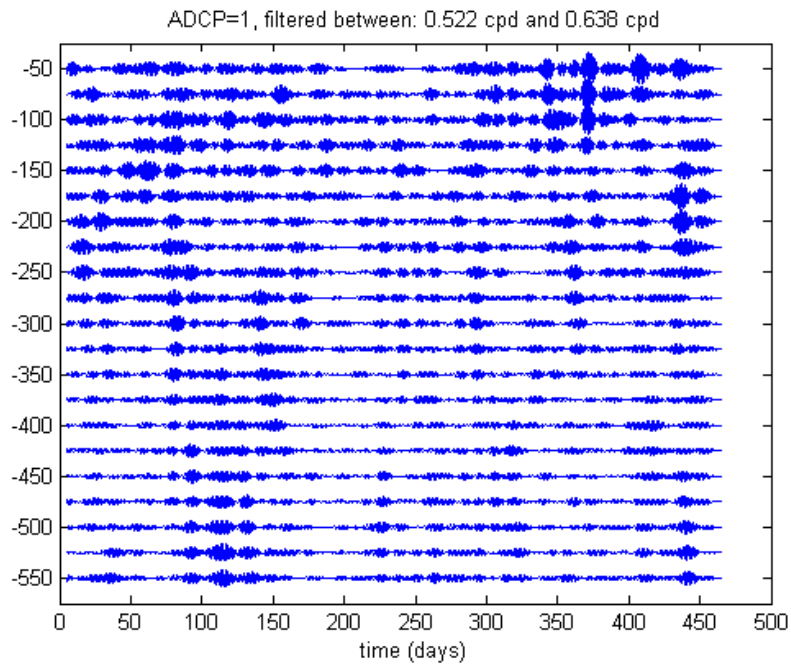


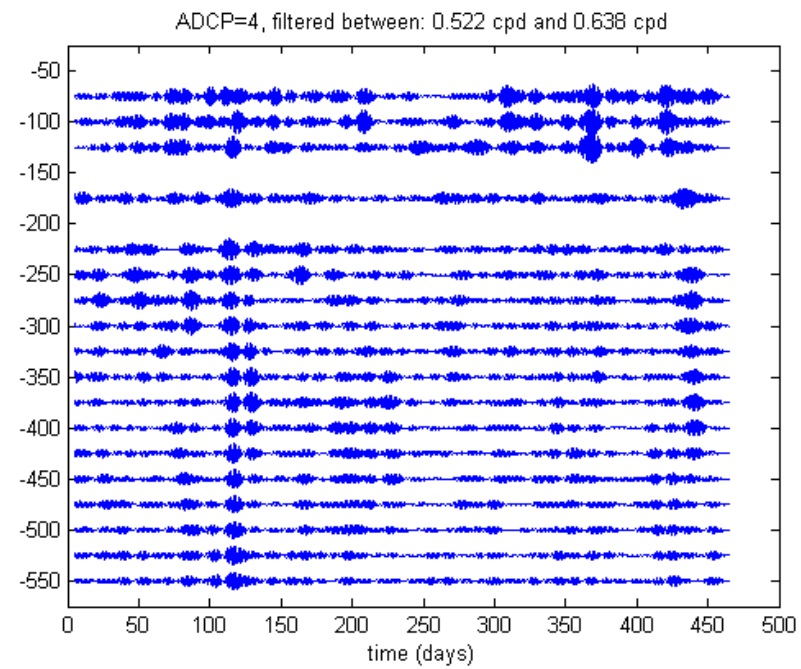
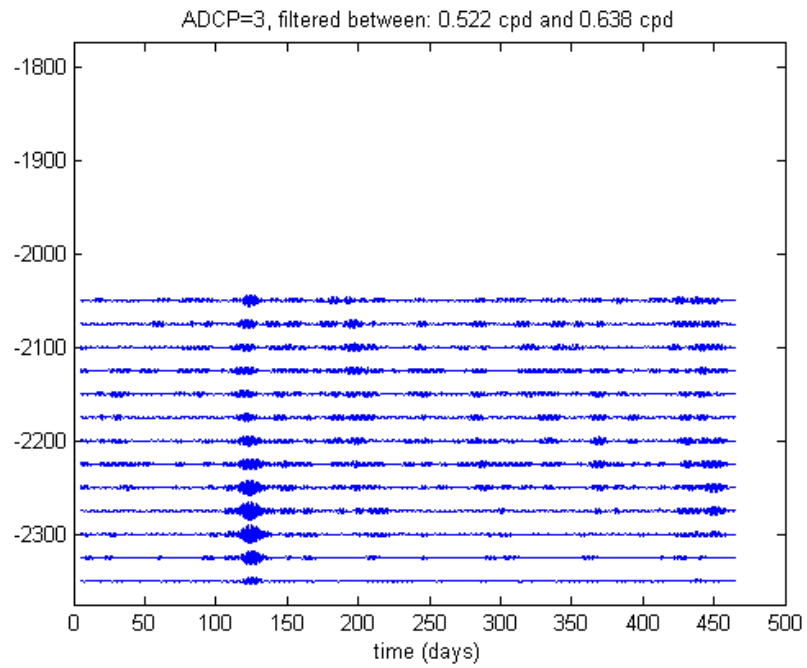


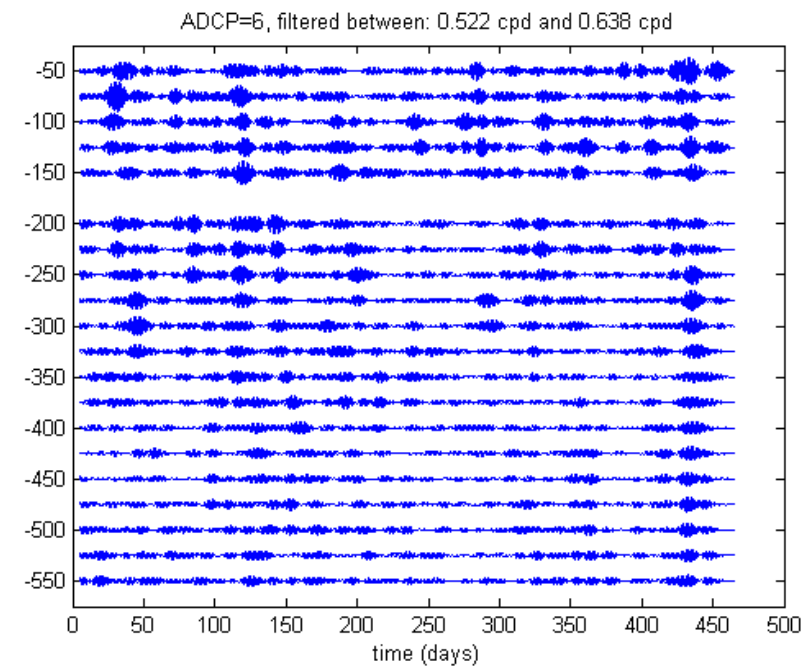
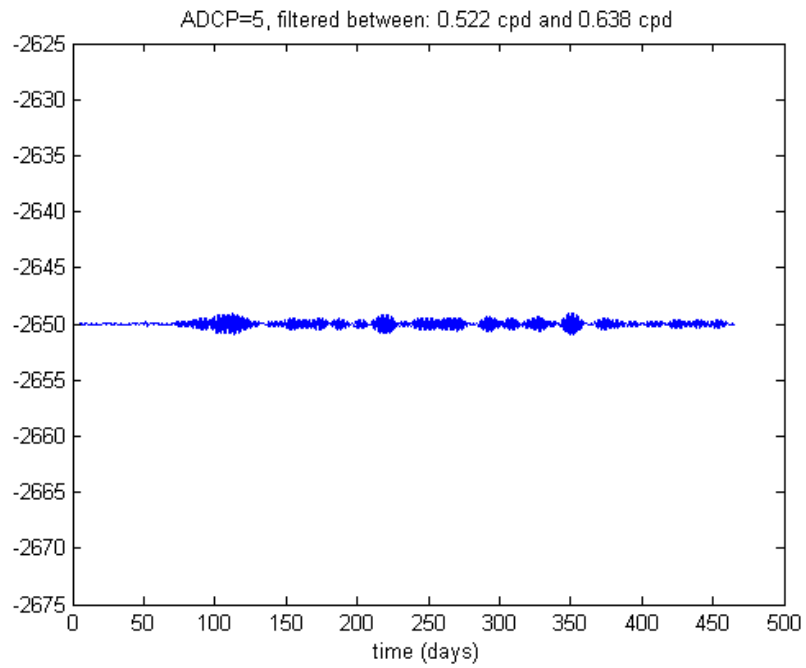




D.2 Meridional velocity (v)

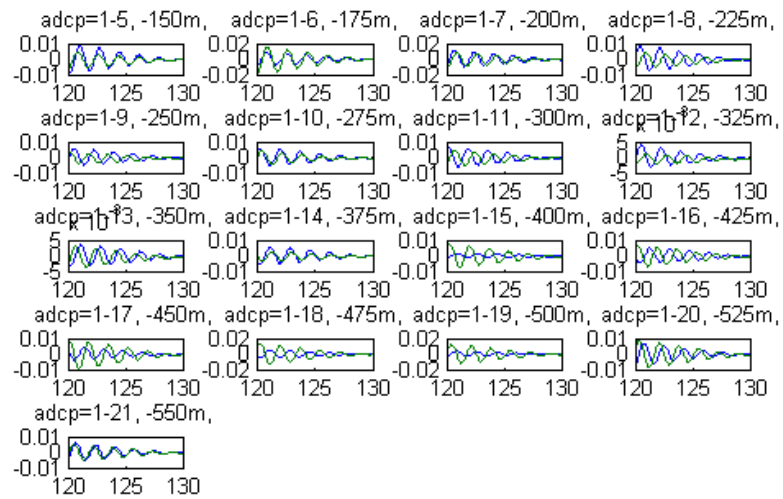


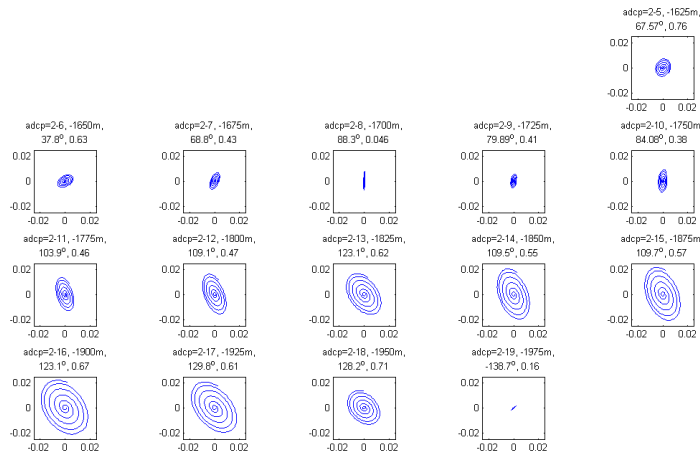
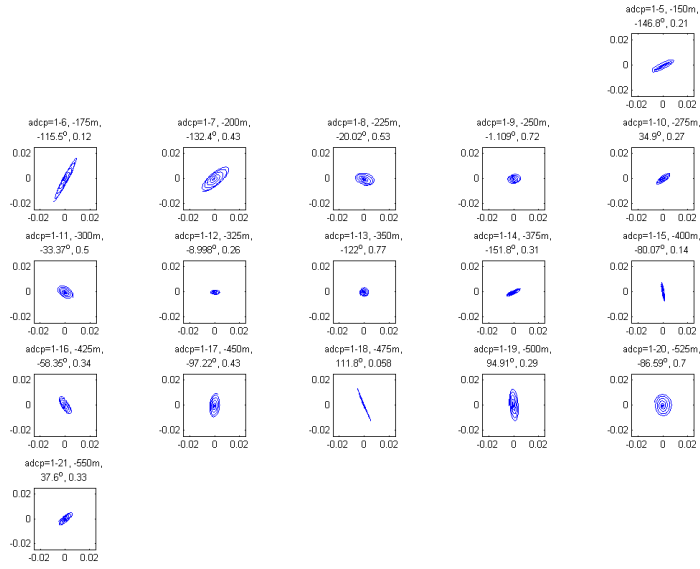


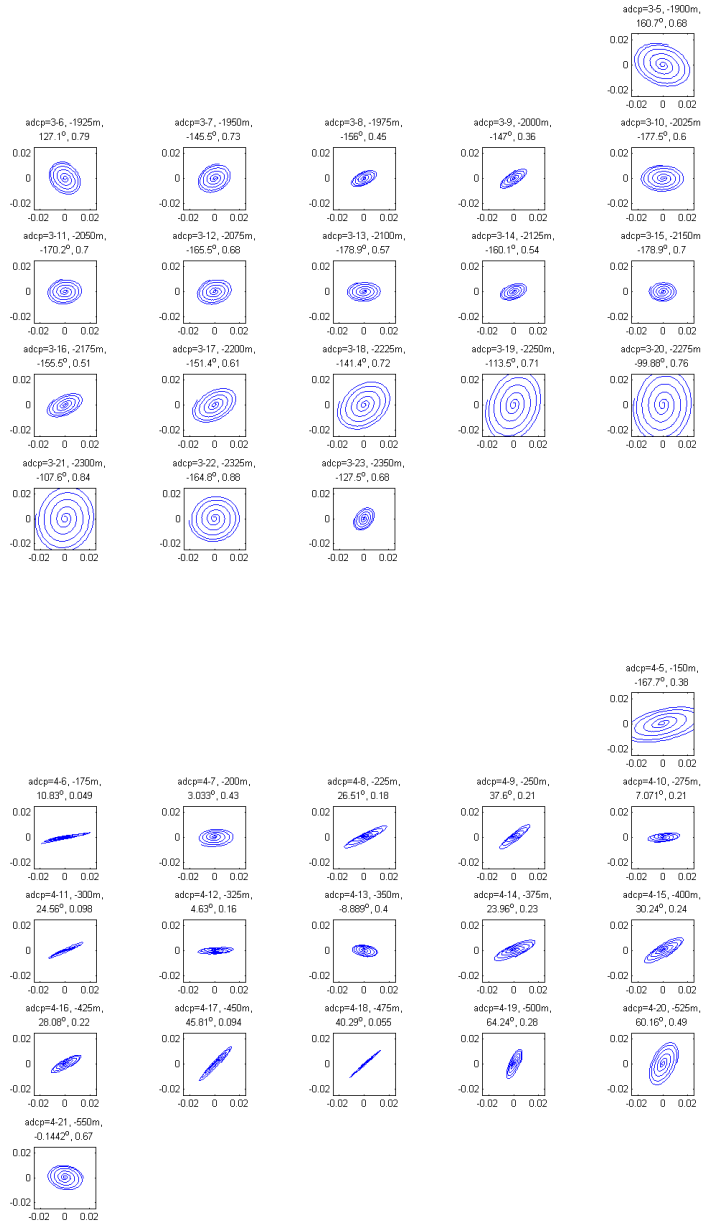


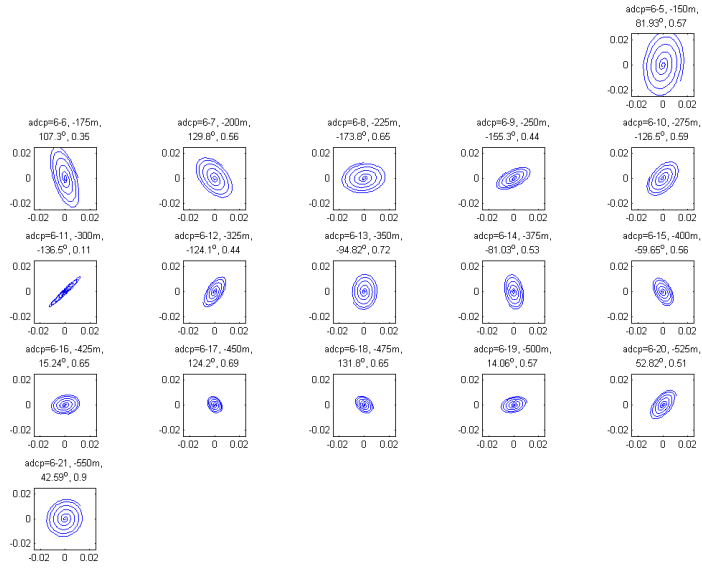
E Hodographs

The hodographs show u (horizontal) versus v in the time domain from day 120 to 130. We calculated the ellipticity, by dividing the length of the minor axis by the length of the major axis. We also determined the angle of the major axis with respect to the horizontal axis in the $u - v$ plane.



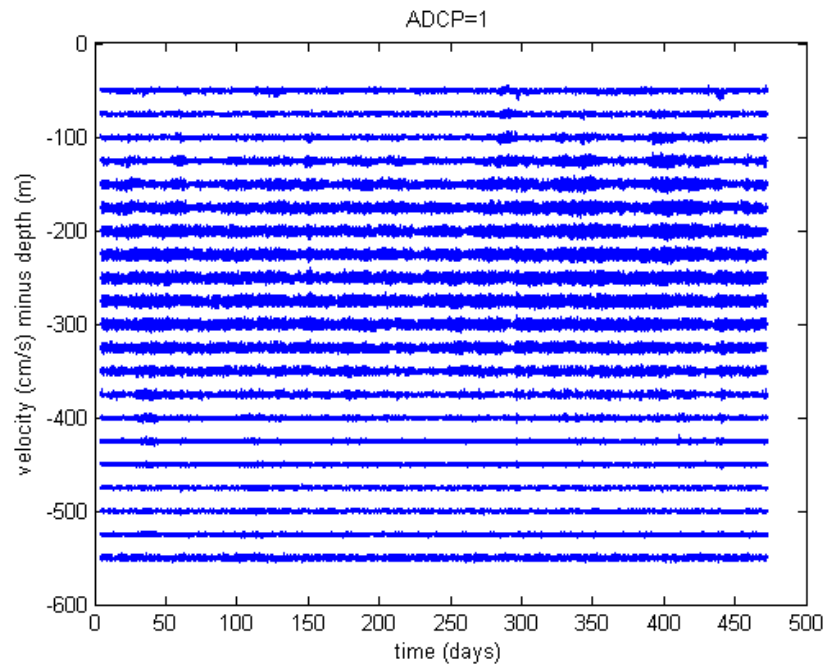


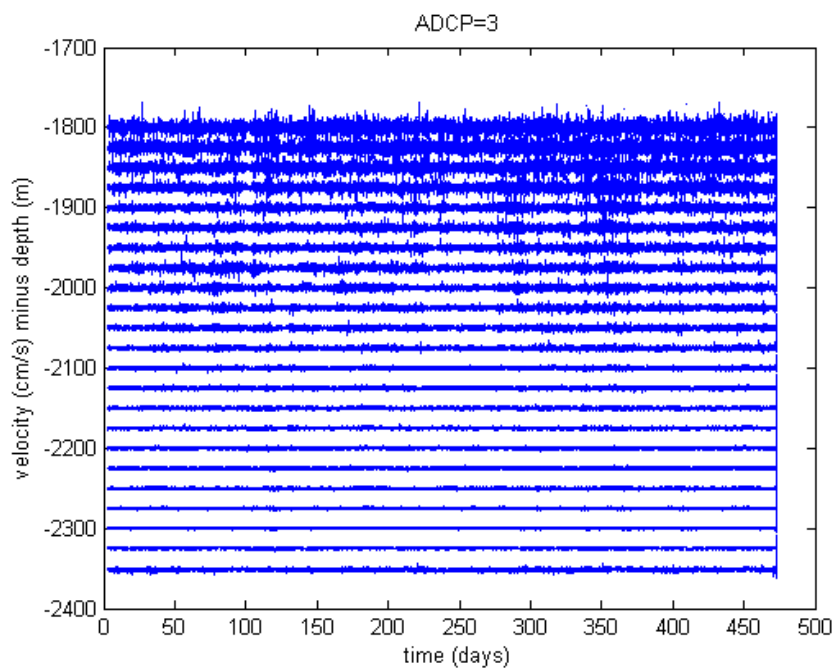
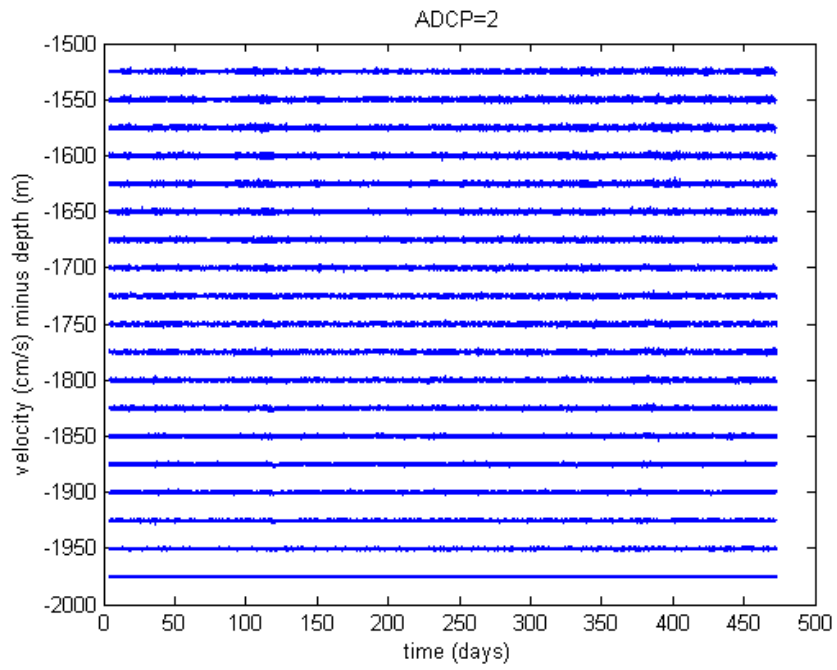


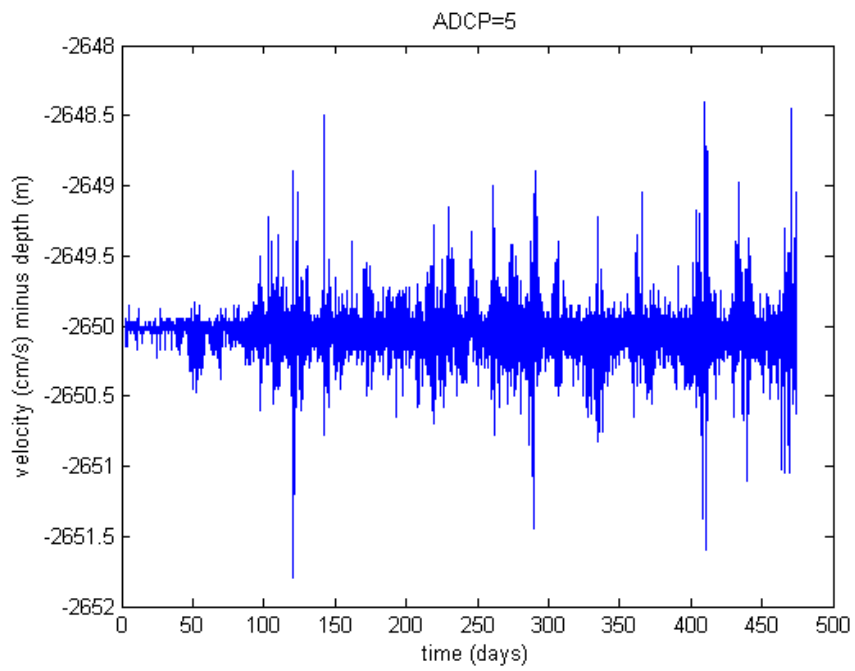
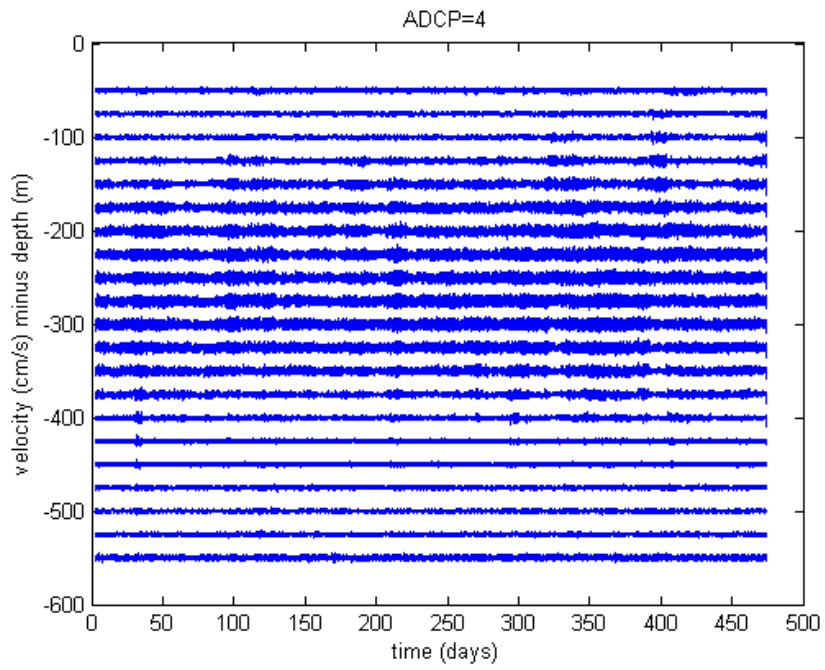


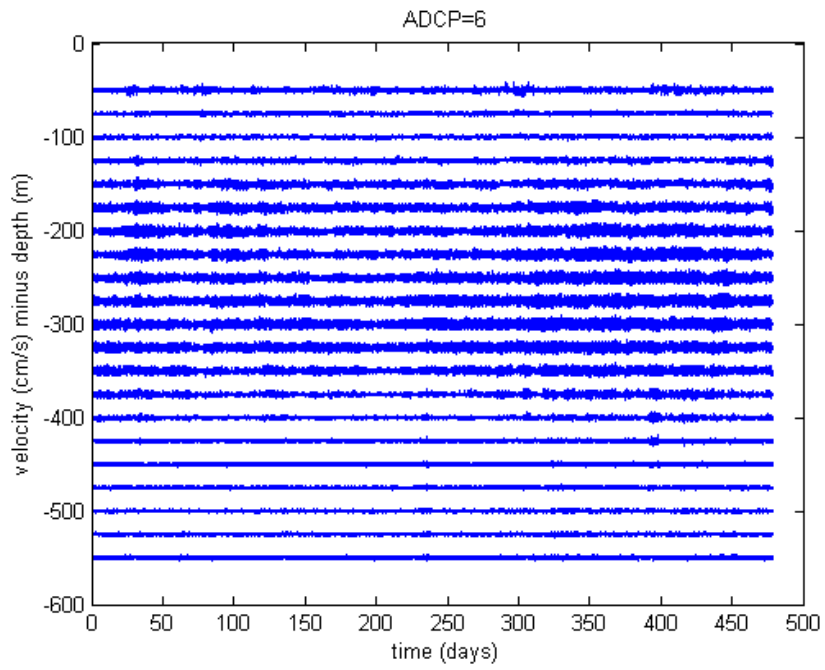
F Vertical current

F.1 Vertical velocity

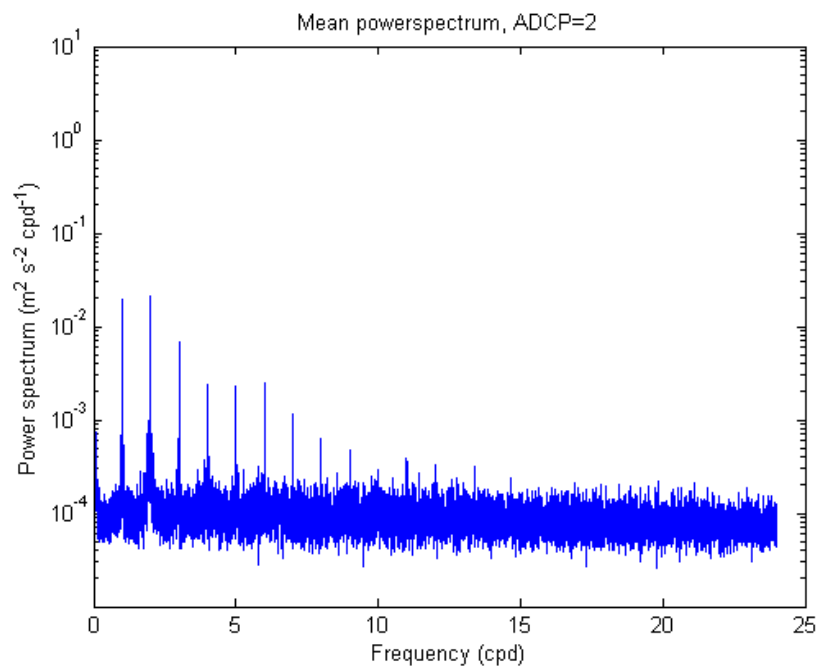
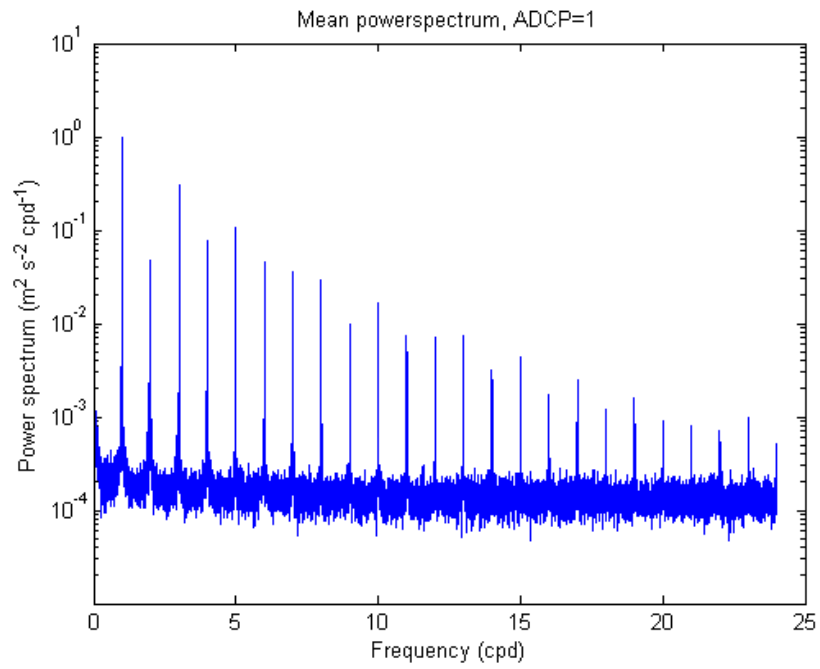


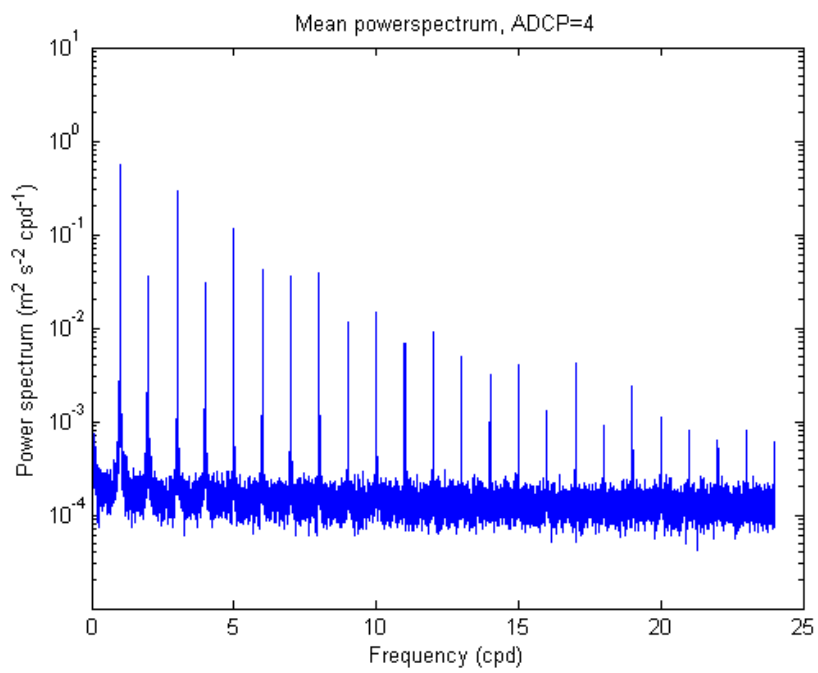
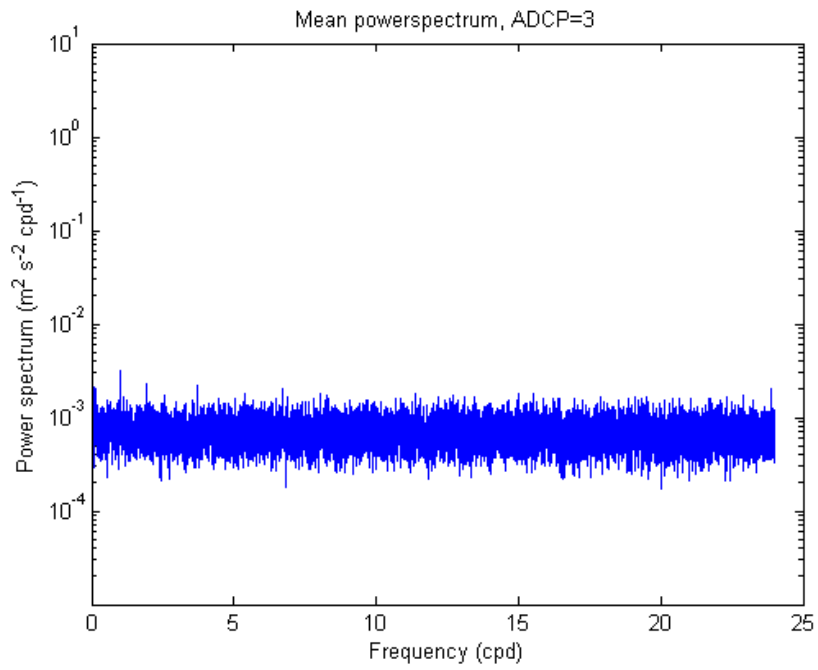


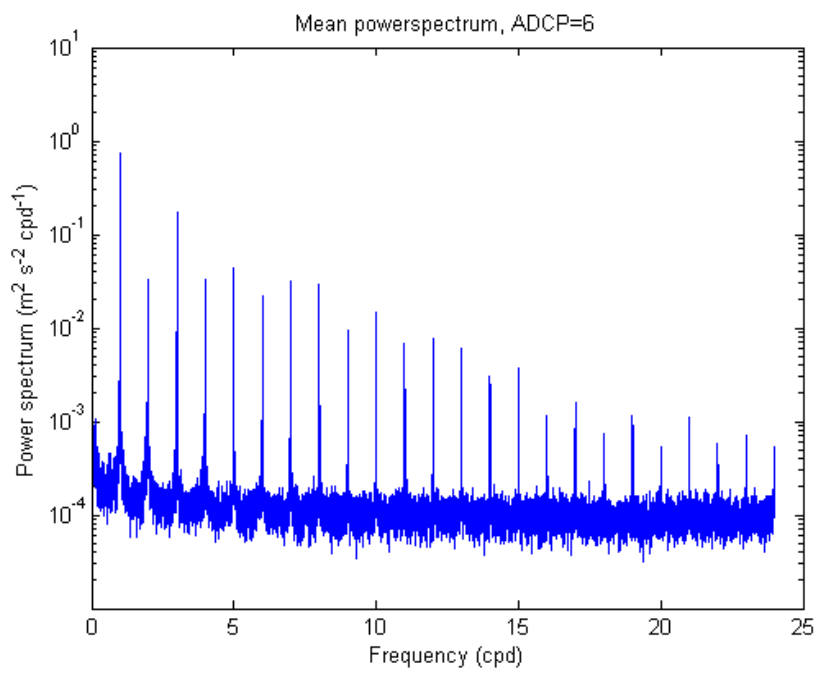
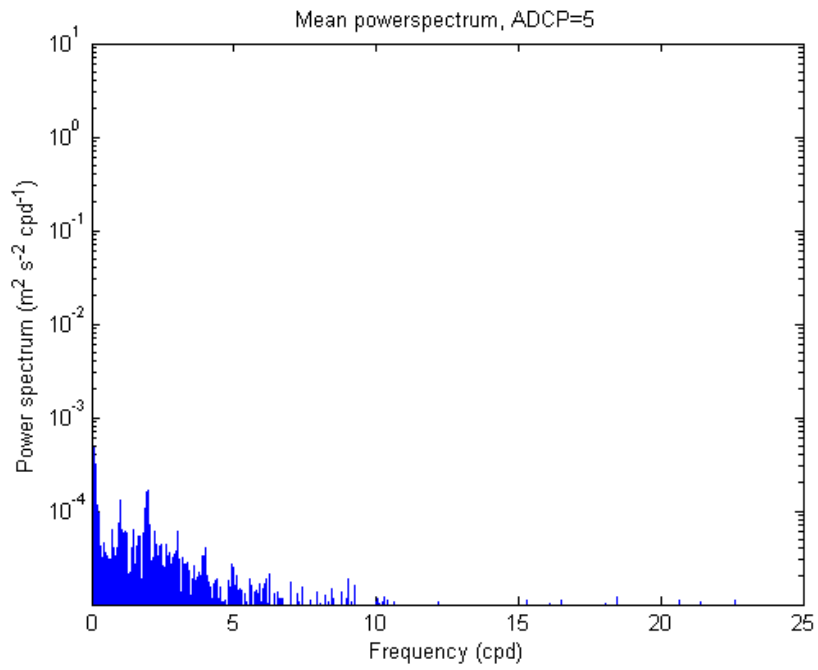




F.2 Vertical spectra





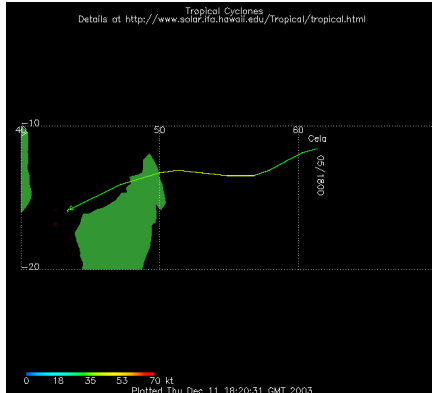


G Extra tables

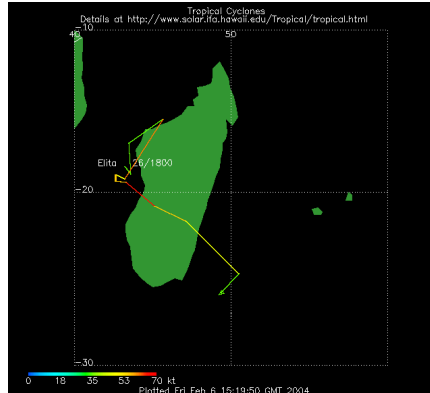
Tidal Component	Period (solar hours)	Description	Nature
M2	12.42	Principal lunar	semi-diurnal
S2	12.00	Principal solar	semi-diurnal
N2	12.66	Larger lunar elliptic	semi-diurnal
K2	11.97	Luni-solar	semi-diurnal
K1	23.93	Luni-solar diurnal	diurnal
O1	25.82	Principal lunar diurnal	diurnal
P1	24.07	Principal solar diurnal	diurnal
Q1	26.87	Larger lunar elliptic	diurnal
MF	327.90	Lunar fortnightly	Long term
MM	661.30	Lunar monthly	Long term
SSA	4383.00	solar semi annual	Long term
M4	6.21		Compound
MS4	6.10		Compound

Table 3: Principal tidal components (source: <http://csep1.phy.ornl.gov/CSEP/OM/NODE31.html>)

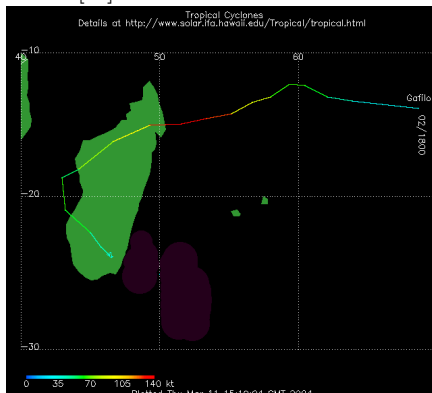
Tropical Cyclone Ceta developed in the South Indian Ocean on the 5th moved across northern Madagascar on the 9th-10th producing torrential rains and maximum sustained winds near 85 km/hr (45 knots or 50 mph).



Tropical Cyclone Elita formed on the 26th in the Mozambique Channel and moved into Madagascar on the 28th. Maximum sustained winds were near 110 km/hr (60 knots or 70 mph) as the cyclone came ashore, along with torrential rains.



Tropical Cyclone Gafilo developed in the South Indian Ocean on the 2nd and struck northern Madagascar on the 7th. Gafilo came ashore near Antalaha with maximum sustained winds near 260 km/hr (140 knots or 160 mph). [...] The cyclone moved back over the Mozambique Channel before coming back across the southern part of the island nation on the 10th. [...]



Tropical Cyclone Ernest developed in the Mozambique Channel between Madagascar and the coast of Mozambique on the 20th. The cyclone reached the coast of southern Madagascar on the 23rd, with maximum sustained winds at the time of land-fall near 100 km/hr (60 mph). [...]

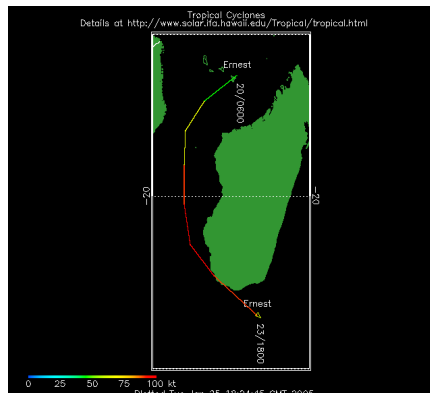


Table 4: Tracks and descriptions of tropical cyclones passing Madagascar (source: <http://www.ncdc.noaa.gov/oa/reports/weather-events.html>)

References

- [1] L. R. M. Maas and F. P. A. Lam. Geometric focusing of internal waves. *Journal of Fluid Mechanics*, 300:1–41, 1995.
- [2] Leo R. Maas, Dominique Benielli, Joel Sommeria, and Frans-Peter A. Lam. Observation of an internal wave attractor in a confined, stably stratified fluid. *Nature*, 388(6642):557–561, 1997.
- [3] A. K. van Veldhoven. The propagation of internal tides in the faeroe-shetland channel. Utrecht Univ., 2000.
- [4] A. M. M. Manders, L. R. M. Maas, and T. Gerkema. Observations of internal tides in the mozambique channel. *Journal of Geophysical Research*, 109:C12034+, December 2004.
- [5] T. Gerkema. Application of an internal tide generation model to baroclinic spring-neap cycles. *Journal of Geophysical Research (Oceans)*, 107:7–1, September 2002.
- [6] P. H. Leblond and L. A. Mysak. *Waves in the ocean*. Elsevier, 1977.
- [7] T. Gerkema and J. T. F. Zimmerman. Interne golven. Diktaat Instituut voor Marien en Atmosferisch onderzoek Utrecht (IMAU), 1999.
- [8] T. Gerkema. Interne getijden en solitonen. *Ned. tijdschrift voor natuurkunde*, 16, 1995.
- [9] H. Ridderinkhof. Cruise report rrs discovery d289b, mozambique channel. Royal NIOZ, 2005.
- [10] David R. Jackett and Trevor J. McDougall. Minimal adjustment of hydrographic profiles to achieve static stability. *Journal of Atmospheric and Oceanic Technology*, 12(2):381–389, 1995.
- [11] B. Cushman-Roisin. *Introduction to geophysical fluid dynamics*. Prentice-Hall, 1994.
- [12] L. R. M. Maas. Wave focusing and ensuing mean flow due to symmetry breaking in rotating fluids. *Journal of Fluid Mechanics*, 437:13–28, June 2001.
- [13] A. M. M. Manders. *Internal wave patterns in enclosed density-stratified and rotating fluids*. PhD thesis, Utrecht Univ., 2003.
- [14] T. Gerkema and V. I. Shrira. Near-inertial waves in the ocean: beyond the "traditional approximation". *Journal of Fluid Mechanics*, 529:195–219, April 2005.
- [15] Hongbo Qi, Roland A. De Szoeko, Clayton A. Paulson, and Charles C. Eriksen. The structure of near-inertial waves during ocean storms. *Journal of Physical Oceanography*, 25(11):2853–2871, 1995.

- [16] Hans van Haren and Claude Millot. Rectilinear and circular inertial motions in the western mediterranean sea. *Deep Sea Research Part I: Oceanographic Research Papers*, 51(11):1441–1455, November 2004.
- [17] T. Gerkema and V. I. Shrira. Near-inertial waves on the nontraditional plane. *Journal of Geophysical Research (Oceans)*, 110:1003+, January 2005.